

國立交通大學
光電工程系暨研究所
博士論文

近簡併共振腔皮秒克爾鎖模雷射之非線性動力學

**Nonlinear dynamics of picosecond Kerr-lens
mode-locked laser around degenerate configurations**

研究生：許智章

指導教授：謝文峰 教授

中華民國九十八年六月

近簡併共振腔皮秒克爾鎖模雷射之非線性動力學

Nonlinear dynamics of picosecond Kerr-lens mode-locked laser around
degenerate configurations

研究生：許智章

Student：Chih-Chang Hsu

指導教授：謝文峰

Advisor：Wen-Feng Hsieh

國立交通大學

光電工程學系暨研究所



**Submitted to Department of Photonics and Institute of Electro-Optical Engineering
College of Electrical Engineering and Computer Science
National Chiao Tung University
in partial Fulfillment of the Requirements
for the Degree of
Doctor of Philosophy
in
Electro-Optical Engineering**

June 2009

Hsinchu, Taiwan, Republic of China

中華民國九十八年六月

誌謝

這漫長攻讀博士學位的過程如今也終於告了一個段落。學位的取得所帶來的不僅僅只是喜悅而且也帶來了自我的肯定。這八年來感謝謝文峰教授在學術研究上的悉心指導，並且在我即將放棄時以其無比的耐心給予我引導與鼓勵，如此師恩著實令人難忘。同時感謝我的父母親、家人以及倍卿，謝謝你們包容我的任性，有你們的支持使我得以無後顧之憂的完成這個學位。感謝好友益志、建邦、耀庭、馬二、阿玖、菟淑，在苦悶的日子裡三不五時的陪我聊天解悶。尤其是益志，畢業口試過程的順利，你可說是功不可沒。

感謝快樂希望的雷射診斷實驗室陪我一起成長。這裡有著太多要感謝的人不論是已畢業或是還未畢業。家弘學長在實驗技巧上的指導及陳慶緒學長於數值模型的建立使我對於實驗觀察的現象能夠有更完善的解釋。在材料量測實驗上，阿笑（盈秀）、穎書、芸佩，因為你們的努力讓我除了雷射動力學領域之外亦能涉足材料光學特性量測領域。黃至賢、博濟、厚仁，每次與你們討論都能讓我有新的領悟與收穫。感謝信民提供一個工研院的兼職工作使我在這半年無斷炊斷糧之虞。還有黃董、維仁、楊松、小豪、晉嘉、小布丁（婉君）等不及細數的快樂希望實驗室成員們，不論是出遊、聚餐、打球、打電動，甚至是做實驗，謝謝你們陪我共同編織出美好的回憶。

最後，感謝所有口試委員所提供的意見讓此論文內容得以更嚴謹更完善，以及國科會研究計畫 NSC 96-2628-E-009-018-MY3 所提供的獎學金及實驗經費讓我能夠順利完成所有的研究。

近簡併共振腔皮秒克爾鎖模雷射之非線性動力學

學生：許智章

指導教授：謝文峰 教授

國立交通大學光電工程學系暨研究所

摘 要

我們研究皮秒克爾鎖模雷射在簡併共振腔架構附近之非線性動態行為。由實驗中我們觀察到無外部調變與回饋控制情況下自啟動克爾鎖模雷射其自啟動行為。從產生雷射後至穩定鎖模期間，雷射輸出功率呈現一短暫且連續不規則輸出（free-running spiking），並且每次持續的時間皆不相同。利用 Grassberger-Procaccia 分析法對其暫態部分做相關維度（correlation dimension）分析，我們得到一非整數值亦即表示此一暫態行為呈現渾沌特性。利用自相關函數對其做進一步分析亦顯示其具有渾沌特徵。我們將此暫態行為等分成數段並計算各段之相關維度，我們發現相關維度由較高的非整數值逐漸減少直到於穩定鎖模區域時相關維度為零。

在皮秒自克爾鎖模鈦藍寶石雷射中我們在簡併共振腔附近觀察到脈衝串列振幅調變。隨泵浦功率的增加脈衝串振幅調變的包絡逐漸由單群分裂成兩群或三群且調變深度亦隨之加深，最後當泵浦功率增加至更高功率，脈衝串振幅調變變成雜亂無序。由於皮秒雷射之脈衝強度遠小於飛秒雷射，故此調變應該不是由高階光固子或色散所造成的。再者脈衝串調變可操作範圍僅 15 微米，雷射共振腔的損耗應該沒

有太大變化，因此調變行為亦非遲緩震盪（relaxation oscillation）所造成。由於產生調變行為的操作區域略為偏離簡併共振腔架構，故可能因雷射晶體中空間不均勻增益所產生的兩組未與縱模相互簡併之高階橫模相互競爭所造成調變行為。

藉由薄片近似（thin slab approximation）我們可以描述一脈衝於共振腔傳播時，共振腔架構對其橫模模態分佈影響。我們使用柯林繞射積分（Collin integral）和考慮自聚焦效應之速率方程式，以數值模擬研究皮秒鎖模雷射於簡併共振腔附近的動態行為。在不考慮自聚焦效應於速率方程式時，我們發現雷射輸出功率隨腔長的變化呈現一功率凹陷的分佈。然而於速率方程式中加入自聚焦效應時，脈衝串的包絡呈現各種狀態，其中包括連續輸出或週期、週期-2 以及不規則狀態。值得注意的是數值模擬結果類似於自啟動克爾鎖模雷射，於自啟動時雷射輸出行為發生於不穩定與連續波輸出操作區域之間。這些現象均與我們在實驗中所觀察所得是一致的。此外，由於起始電場之振幅與相位初始值來自於自發輻射，於不同次模擬結果，此短暫且連續不規則輸出持續時間不完全相同且呈現一指數函數遞減分布趨勢。其回歸映像（return map）呈現出在起始時具有奇異吸子的渾沌態，隨時間演化轉變成準週期態最後收斂於穩定態。理論模擬結果顯示自啟動鎖模從雷射於渾沌態轉為穩定鎖模態之自適行為應由自聚焦效應所造成。

Nonlinear dynamics of picosecond Kerr-lens mode-locked laser around the degenerate configurations

Student : Chih-Chang Hsu

Advisor : Prof. Wen-Feng Hsieh

Department of Photonics & Institute of Electro-Optical Engineering
National Chiao Tung University

ABSTRACT

We experimentally observed the transient state from the laser starting to reaching a stable mode-locking (ML) state in a self-starting Kerr-lens mode-locked Ti:sapphire laser without external modulation and feedback control. By Grassberger-Procaccia analysis for the transient state, the correlation dimension of the transient state is a non-integer which implies it is a chaotic state. The chaotic characteristic can be further confirmed by observing the revivals of the autocorrelation function for long delay time.

Pulse-train modulation was observed in this laser with pump-power dependence when it was operated around the degenerate cavity configuration. By increasing the optical pumping power, the envelope of periodic amplitude modulation splits into two or three clusters with enhanced modulation depth, and the amplitude modulation eventually becomes disordered at higher pump power. The amplitude modulation may be supported by exciting two sets of non-degenerate longitudinally mode-locked supermodes due to spatially inhomogeneous gain modulation in the Ti:sapphire crystal.

We also numerically studied suppressing chaos to reaching completely mode-locking in this self-starting Kerr-lens mode-locked (KLM) laser. By thin slab approximation, we can describe transverse effect of a pulse propagates in a resonator. Based on Fox-Li's approach, we used the Collins integral and rate equations with and without the self-focusing effect, we found without the self-focusing effect typical laser output and the feature of a power dip agrees with the observation of experiment for all calculated cavity configurations around the degeneracy at various pump powers. However, by adding the self-focusing effect, the time evolution of the pulse-train envelope presents various states including continuous wave or periodic state and instability such as period, period-2, and irregular states. The simulated self-starting KLM output, which possesses transient irregularity before reaching a constant amplitude output, occurs between the instability and continuous wave regions. The different runs of the simulated self-starting from the spontaneous emission reveal the buildup time of mode-locking not only is sensitive to the initial condition but also presents the distribution with exponential decay. Its return map presents chaotic state with a strange attractor in the initial stage. It transits to the quasi-periodic state and finally converges to a fixed point with time evolution. The theoretical simulation reveals that the self-focusing effect is responsible for the self-adaptation.

Contents

Abstract in Chinese.....	I
Abstract in English.....	III
Contents.....	V
List of Figures.....	VII
Chapter 1 Introduction.....	1
1.1 Degenerate cavity and iterative map.....	1
1.1-1 Degenerate cavities.....	1
1.1-2 Iterative map.....	2
1.2 Self-starting of Kerr-lens mode-locked laser.....	5
1.3 Pulse-train amplitude modulation in a picosecond KLM laser.....	7
1.4 Aim of this research.....	9
1.5 Organization of this dissertation.....	10
Chapter 2 Experimentals.....	16
2.1 Experimental construction for a symmetric KLM laser.....	16
2.2 The measurement of self-starting Kerr-lens mode-locking	18
2.3 The observation of pulse-train amplitude modulation	18
2.4 The measurement of spatio-temporal instability	19
Chapter 3 Numerical model	22
3.1 Thin slab approximation	22
3.2 Huygen's integral and ABCD matrix	26
3.3 Simulation model of the KLM laser	28

Chapter 4 Results and Discussion	35
4.1 Nonlinear dynamics analysis of self-starting KLM laser.....	37
4.2 Pulse train amplitude modulation.....	46
4.3 Spatial-temporal instability.....	56
Chapter 5 Conclusions and Prospective	64
5.1 Conclusions.....	64
5.2 Prospective.....	66
Resume	68
Publication list	68



List of Figures

Fig. 2-1 The schematic experimental setup of the Kerr-lens mode-locking Ti:sapphire laser.....	17
Fig. 2-2 The beam pattern around the 1/3-degenerate cavity configuration.....	20
Fig. 3-1 A traveling pulse or “slab” of optical radiation propagating in the z direction.....	23
Fig. 3-2 The sketch of an iterated period optical (lensguide) system.....	25
Fig. 3-3 The sketch of one-dimension Huygens’s integral.....	26
Fig. 3-4 The sketch of the optical ray through an ABCD paraxial system.....	28
Fig. 3-5 Schematic of an equivalent four-mirror cavity configuration.....	29
Fig. 4-1 The output clusters of the self-starting pulse train on the oscilloscope with 5 W pumped.....	37
Fig. 4-2 The calculated $\log [C(r)]/\log(r)$ versus $\log(r)$ with embedding dimension D_e from 2 to 12 by the GPA.....	39
Fig. 4-3 The simulation results of the laser output power around the degenerate cavity configuration.....	41
Fig. 4-4 The time evolution of the correlation dimension of the observed and the return map of simulated output power.....	43
Fig. 4-5 Distribution of finding $1/A_{eff}$, initiation and after 10,000 round trips, for a cavity tuning range of $70 \mu\text{m}$	46
Fig. 4-6 Power-dependent mode-locked pulse-train modulations.....	47
Fig. 4-7 The expanded power spectra of different modulation state of Fig. 4-6 around the central frequency 93.3 MHz.....	49
Fig. 4-8 The simultaneous intensities of the laser at two transversal positions labeled A and B in the inset of Fig. 2-2.....	51

Fig. 4-9 The simulated evolution of output power with changing pump power from 4 W to 5 W with and without Kerr effect.....56

Fig. 4-10 The simulated numerical evolution of laser without self-focusing effect ($n_2 = 0$).....57

Fig. 4-11 The temporal evolution of the intensity profiles of perio-2 pulse-train amplitude modulation.....58

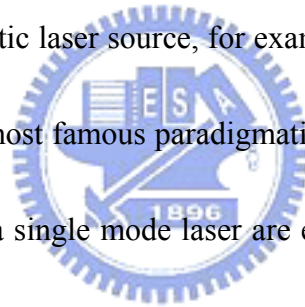
Fig. 4-12 The evolution of laser from two different runs show both starting from the irregular spiking before reaching a periodic (KLM) state around $r_1=53.625$ mm.....60

Fig. 4-13 The histogram of the calculated buildup times of self-starting mode-locking (solid squares) with an exponential fitting curve (dash line).....60



Chapter 1 Introduction

Since the laser came on the scene, the rich nonlinear behaviors have been investigated intensively in laser systems. The researchers proposed various models to describe the laser instabilities [1, 2]. The problems such as spontaneous irregular pulsing, modulation instabilities, and unstable mode patterns etc., coming from intrinsic nonlinearities of the lasers are the topics of laser dynamics [3]. For applications, one prefers to operate the laser with stable continuous-wave (CW) or periodic pulsing while sometimes one may use a chaotic laser source, for example, in chaotic communications. When Haken constructed the most famous paradigmatic model [4] in 1975 in which the Maxwell-Bloch equations for a single mode laser are equivalent to those of the Lorenz model for fluids, regarding as the cornerstone in laser dynamics, this field becomes popular until today.



1.1 Degenerate cavities and iterative map

1.1-1 Degenerate cavities

The resonance condition for a standing-wave is the phase shift for total round-trip must be $2n\pi$, where n is an integer. The total phase shift from one end of cavity to the other end includes kL and Gouy phase shift terms, where $k = 2\pi/\lambda$ is the wave number, λ is wavelength of laser, and the Gouy phase is an additional phase introduced by a

paraxial wave function substitution for an (n,m)-th order Hermite-Gaussian mode in mathematics. The total Gouy phase shift of a laser cavity with cavity length L is given in terms of the g-parameters by the formula

$$(n + m + 1) \cos^{-1}(\pm \sqrt{g_1 g_2}), \quad (1.1)$$

where n and m are the mode numbers in the x- and y-axes, respectively. Because the Gouy phase shift depends on Hermite-Gaussian mode numbers, different transverse modes of a stable Gaussian resonator have different resonance frequencies. Therefore the resonance frequency of Hermite-Gaussian (n,m) mode is given by

$$\nu_{n,m,q} = \frac{c}{2L} \left(q + \frac{n+m+1}{\pi} \cos^{-1} \sqrt{g_1 g_2} \right), \quad (1.2)$$

where q is the longitudinal mode number. From Eq. (1.2), we can define the longitudinal mode spacing $\nu_l = c/2L$, and the transverse mode spacing $\nu_t = (\nu_l/\pi) \cos^{-1}[(g_1 g_2)^{1/2}]$. Here we denote the terms as 1/2-, 1/3-, 1/4-degenerate configurations because the configurations with $g_1 g_2 = 0, 1/4, \text{ and } 1/2$ correspond to $\nu_l/\nu_t = 1/2, 1/3, \text{ and } 1/4$, respectively. In these configurations, the fundamental modes may be degenerate with other high-order transverse modes which obey Eq. (1.2). The degenerate modes may through the mode competition or the mode beating result in instability of laser output [5, 6]. Therefore, the degenerate cavity is a good choice to investigate laser dynamics.

1.1-2 Iterative map

The iterative map is a mathematical tool to study the nonlinear dynamics. The study of a continuous system can be reduced to a discrete time system on a surface of section transverse to the flow. We take the time period with the round-trip time of the laser cavity, and then the iterative map can be constructed. Applying the ABCD law in a two mirror cavity with the reference plane at one of the mirrors [7], the q-parameter ($1/q = 1/R - i\lambda/\pi w^2$) of the Gaussian beam of the (n+1)-th round trip to the n-th one can be written as

$$\begin{cases} w_{n+1} = f_1(w_n, R_n) = w_n \sqrt{(A + B/R_n)^2 + ((\lambda/\pi w_n^2))^2 B^2}, \\ R_{n+1} = f_2(w_n, R_n) = \frac{(A + B/R_n)^2 + ((\lambda/\pi w_n^2))^2 B^2}{(A + B/R_n)(C + D/R_n) + ((\lambda/\pi w_n^2))^2 BD}, \end{cases} \quad (1.5)$$

where w is the spot size and R is the radius of curvature. This map belongs to the conservative one because the resonator is lossless. The stability condition $|Tr(J_p)| < 2$ depends only on the trace $Tr(J_p)$ with the Jacobian matrix J_p evaluated at the studied fixed point. The stability condition depends on the residue that defined as $Res = \frac{1}{4}(2 - Tr(J_p)) = \sin^2(\theta/2)$, where θ is the phase shift per iteration of the map. For $0 < Res < 1$, the system is stable that corresponds to the conventional geometric stable regime $0 < g_1 g_2 < 1$, where $g_{1,2} = (1 - d/R_{1,2})$ of the two-mirror cavity is the so-called g-parameter of the optical cavity [8, 9]. For $Res < 0$ and $Res > 1$, the system is unstable. By applying the Greene's residue theorem, Wei et al. [10, 11] indicated that the special case of $Res = 0, 1, 3/4, 1/2$ correspond to the degenerate cavities or the

so-called low-order resonances that correspond to the cavity configuration with a specific low fraction g_1g_2 parameter. For a simple two-mirror cavity, these special condition correspond to $g_1g_2 = 0$ and 1 for $\text{Res} = 0$; $g_1g_2 = 1/2$ for $\text{Res} = 1$; $g_1g_2 = 1/4$ and $3/4$ for $\text{Res} = 3/4$ and $g_1g_2 = (2 \pm \sqrt{2})/4$ for $\text{Res} = 1/2$, respectively. It is worth noting that these configurations are very sensitive to any perturbation in the laser cavity. Therefore, the laser will present various dynamic behaviors when nonlinear effect exists in a laser system [7, 10, 11].

The dynamics depending on the cavity configuration has been studied in a Kerr-lens mode locked (KLM) Ti-sapphire laser [11]. When the optical Kerr effect was considered as the nonlinear dynamical parameter, optical bistability and multiple-period bifurcation were numerically demonstrated. From the guidance, some peculiar phenomena were found by using an end-pumped Nd:YVO₄ laser under small-size pumping that pump size is smaller than the waist of the cold cavity [12-16]. A supermode or superposition of phase-locked degenerate transverse modes can be formed with relatively low lasing threshold, shrunken beam waist [13] and operation of a stable CW bottle beam [14, 15] were observed. However, only the temporal chaotic state was observed for the cavity configurations that were slightly shorter than the degenerates and the spatio-temporal chaotic state for those slightly longer than the degenerates [16].

1.2 Self-starting of Kerr-lens mode-locked laser

In solid state mode-locked (ML) lasers, the chaotic behavior of the self-mode locking or the Kerr-lens mode locking (KLM) Ti:sapphire lasers, due to the significant optical Kerr effect (OKE), had also been investigated since the invention of KLM Ti:sapphire laser in 1991 by Spence et al. that requires a mechanical perturbation to start the mode locking [17]. Later, self-starting Kerr-lens mode locking (SSKLM) was shown achievable in this laser, either with or without group velocity compensation [18, 19] in a narrower tuning region close to the boundary of spatio-temporal chaotic and CW states [20]. The basic mechanism underlying pulse formation in these self-mode locked lasers has been attributed to self-focusing caused by Kerr nonlinearity to modulate the cavity gain or loss in terms of soft-aperture or hard-aperture Kerr-lens mode locking [21, 22], respectively. For the soft-aperture systems, however, because the only mechanism to restrict higher-order transverse modes is the modal profile of the gain and because Kerr-lens mode locking itself is intrinsically a nonlinear phenomenon, it is not surprising that such systems may exhibit more complicated transverse dynamics. Recently, period doubling [23, 24] and tripling [24, 25] of soft-aperture Kerr-lens mode locked Ti:sapphire lasers were observed by operation of the resonators in specific cavity configurations and were explained in terms of the total mode locking of TEM_{00} and higher-order modes [26, 27].

Although the dynamic processes of the self-starting KLM lasers have been extensively investigated in early time in which starting from relaxation oscillation through a short period intermediate free running to reach a final stable KLM were generally reported [28], many efforts concerning about the routes to chaos after the lasers being operated with the KLM state were reported, e.g., Bolton et al. [29], and our previous report [20]. Phase plot of period, quasiperiodic, and chaotic regimes shows as a function of pump power and insertion of prism [21]. However, to the best of our knowledge, self-adaptation from transient spiking to complete mode-locking with neither external modulation [30-32] nor feedback control [33-35] had not been examined in laser systems.



Furthermore, a self-adapting or self-adjusting system is an adjustable system whose control parameters are adjusted by the forcing dependent only on the system itself [36]. Such systems have been found to adapt to the edge of chaos, which is the boundary of chaos and the order state [36, 37]. Using a logistic map as an example [36], it had been found that the parameter leaves the chaotic regime and there is a high probability of finding the parameter at the boundary between periodicity and chaos when the control parameter of the system is not constant in time, but varies much more slowly than the dynamical variables. These phenomena are ubiquitous in nature; for example, long-range fitness correlations have been detected during the adaptive process

in RNA viruses [38]. In addition, models of coupled neurons with self-adjusting coupling strengths had been found to exhibit robust synchronization [39] and suppression of chaos [40]. The process of self-starting KLM is very much like self-adapting phenomenon.

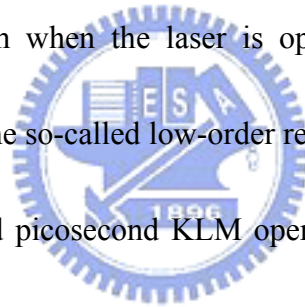
1.3 Pulse-train amplitude modulation in a picosecond KLM laser

Self-mode-locked lasers due to KLM have become the light sources of high-bandwidth ultrashort pulses and been applied to various fields. Recently, the supercontinuum (SC) or white light generation has been demonstrated by injecting the high peak power laser pulses into a photonic crystal fiber (PCF) [41]. By operating the mode-locked Ti:sapphire laser in a pulse-train amplitude modulation mode, the so-called self-Q-switched mode [42] to enhance peak power, the fluctuating structure of SC spectrum can be suppressed significantly [43]. This Q-switching mode-locking pulse train with low repetition rate is very useful for preventing thermal heating in Z-scan and nonlinear optical measurements [44-46].

The solid-state laser media that usually have sufficient long gain relaxation time as compared with the cavity relaxation time are susceptible to intensity spiking and exhibit self-Q-switching phenomena. Accordingly, introducing extra loss in the laser cavity such as saturable absorbers or semiconductor saturable absorber mirrors (SESAM) can generate self-Q-switching, Q-switched mode-locking (QML), and even CW

mode-locked laser pulses [47, 48]. Although the gain relaxation time of Ti:sapphire laser ($3.2 \mu\text{s}$) is larger than the cavity relaxation time ($\sim 10 \text{ ns}$), the mode-locked pulse train in a femtosecond (fs) Ti:sapphire laser can be amplitude modulated by high-order spatial transverse modes [42, 49, 50] or high-order solitons [51] without saturable absorbers. By controlling intracavity hard aperture [49] or operating parameter of the cavity, such as moving spherical mirror or translating prism [42, 49, 50], the intensity dependence of the transverse distribution of the laser beam caused by self-focusing imposes a strong limit on the aperture diameter. When the size of an intracavity slit is reduced below its optimal value for stable mode-locking, the output pulses of the KLM Ti:sapphire laser transform into a regime characterized by periodic pulse-train amplitude modulations as a kind of repetitive self-Q-switching. The modulation period increased and amplitude modulation could deepen to almost 100 percent as the slit width was decreased further [49]. The period of self-Q-switching depends on distance between the folding mirrors, which essentially determine the stability of resonator, and increases with increasing the distance between one of folding mirrors and the closer face of the Ti:sapphire crystal [50]. Among them, the high-order transverse modes, strong Kerr effect due to the ultrashort pulse width, and the group velocity dispersion (GVD) compensation should be responsible to the mode-locked pulse-train modulation in the fs Ti:sapphire lasers.

In contrast, due to the relatively low peak intensity in picosecond (ps) KLM lasers, the strength of Kerr effect is reduced and therefore the pulse-train modulation should occur more difficult than that in fs-KLM lasers. However, because the mode locking mechanism of the KLM laser is due to the self-amplitude or self-gain modulation resulting from the self-focused light by hard or soft aperture effect, the smaller pumped beam spot size than the cold cavity beam one in the gain medium leads to the KLM mode resonating more easily than the CW mode. In an axially tightly-focused pumped laser, it is easier to excite the higher-order transverse modes to extract more stored energy from the gain medium when the laser is operated in the degenerate cavity configurations [24] that have the so-called low-order resonance [8]. The beam patterns observed for both the CW and picosecond KLM operations in the soft aperture KLM regions are no longer pure fundamental Gaussian modes [24]. Due to the competition of transverse modes, the nonlinear dynamics and irregular pulsing have been observed in Nd:YVO₄ lasers [16] and Ti:sapphire lasers [20] operated around the degeneration configurations. The slow amplitude modulation of mode-locked pulse train in the ps-soft-aperture self-mode-locked Ti:sapphire laser around the 1/3-degenerate configuration, which corresponds to the 1/4-fractional low-order resonance, may not only result from the competition of longitudinal modes but also transverse modes.



1.4 Aim of this research

In this research, we will investigate experimentally the dynamic processes of self-starting KLM which begin with the transient chaotic state and finally suppression of chaos to become a stable CW-ML state and the periodic amplitude modulation of ps-mode-locking pulses occurring around the 1/3-degenerate configuration.

We will also employ the numerical model which consider the transverse wave front of a pulse propagating in the cavity to investigate numerically the dynamics behaviors of a picosecond KLM Ti:sapphire laser around the degenerate-cavity configurations. Based on the Fox-Li approach, using the Collin's integral with rate equation including the self-focusing effect, the simulation results reveal that the self-focusing effect is responsible for the dynamics of this laser system that evolves from the chaotic state with a strange attractor to a metastable periodic state and then converges to a fixed point, the CW-ML state. The slow amplitude modulation of mode-locked pulse train in the ps-soft-aperture self-mode-locked Ti:sapphire laser depends upon the optical pumping power. As the pump power increases, the envelope of periodic modulation will split into two or three clusters, and the laser eventually turns into disorder modulation as further increasing the pump power.

1.5 Organization of this dissertation

In this dissertation, it will introduce the experimental setup and the measurement of the self-starting mode-locking, pulse train amplitude modulation and spatio-temporal

instability in Chapter 2. And then it will introduce the simulation model which used the Huygens's integral and rate equation with optical Kerr-effect in Chapter 3. We will discuss our experimental and simulated results which are nonlinear dynamics analysis of self-starting KLM laser, pulse train amplitude modulation and spatial-temporal instability in Chapter 4. Finally, in Chapter 5 it will state the conclusions and the give suggestions for future works.



References

- [1] C. L. Tang, H. Statz, and G. deMars, *J. Appl. Phys.* **34**, 2289 (1963).
- [2] A. Z. Grazyuk, and A. N. Oraevskii, *Quantum Electronics and Coherent Light* (Academic Press, New York, 1964).
- [3] C. O. Weiss, and R. Vilaseca, *Dynamics of Lasers* (Weinheim; New York; Basel;Cambridge: VCH, 1991).
- [4] H. Haken, *Phys. Lett. A* **53**, 77 (1975).
- [5] L. A. Lugiato, G. L. Oppo, J. R. Tredicce, L. M. Narducci, and M. A. Pernigo, *J. Opt. Soc. Am. B* **7**, 1019 (1990).
- [6] J. R. Tredicce, E. J. Quel, A. M. Ghazzawi, C. Green, M. A. Pernigo, L. M. Narducci, and L. A. Lugiato, *Phys. Rev. Lett.* **62**, 1274 (1989).
- [7] M. D. Wei, W. F. Hsieh, and C. C. Sung, *Opt. Commun.* **146**, 201 (1998).
- [8] J. M. Greene, *J. Math. Phys.* **20**, 1183 (1979).
- [9] J. M. Greene, R. S. Mackay, F. Vivaldi, and M. J. Feigenbaum, *Physica D* **3**, 468 (1981).
- [10] M. D. Wei, and W. F. Hsieh, *Opt. Commun.* **168**, 161 (1999).
- [11] M. D. Wei, and W. F. Hsieh, *J. Opt. Soc. Am. B* **17**, 1335 (2000).
- [12] H. H. Wu, and W. F. Hsieh, *J. Opt. Soc. Am. B* **18**, 7 (2001).

- [13] H. H. Wu, C. C. Sheu, T. W. Chen, M. D. Wei, and W. F. Hsieh, *Opt. Commun.* **165**, 225 (1999).
- [14] P. T. Tai, W. F. Hsieh, and C. H. Chen, *Opt. Express* **12**, 5827 (2004).
- [15] P. T. Tai, and W. F. Hsieh, *Opt. Express* **13**, 1679 (2005).
- [16] C. H. Chen, P. T. Tai, and W. F. Hsieh, *Opt. Commun.* **241**, 145 (2004).
- [17] D. E. Spence, P. N. Kean, and W. Sibbett, *Opt. Lett.* **16**, 42 (1991).
- [18] J. M. Shieh, F. Ganikhanov, K. H. Lin, W. F. Hsieh, and C. L. Pan, *J. Opt. Soc. Am. B* **12**, 945 (1995).
- [19] D. G. Juang, Y. C. Chen, S. H. Hsu, K. H. Lin, and W. F. Hsieh, *J. Opt. Soc. Am. B* **14**, 2116 (1997).
- [20] J. H. Lin, and W. F. Hsieh, *Opt. Commun.* **225**, 393 (2003).
- [21] T. Brabec, C. Spielmann, P. F. Curley, and F. Krausz, *Opt. Lett.* **17**, 1292 (1992).
- [22] T. Brabec, P. F. Curley, C. Spielmann, E. Wintner, and A. J. Schmidt, *J. Opt. Soc. Am. B* **10**, 1029 (1993).
- [23] D. Cote, and H. M. van Driel, *Opt. Lett.* **23**, 715 (1998).
- [24] J. H. Lin, M. D. Wei, and W. F. Hsieh, *J. Opt. Soc. Am. B* **18**, 1069 (2001).
- [25] S. R. Bolton, R. A. Jenks, and C. N. Elkinton, *J. Opt. Soc. Am. B* **16**, 339 (1999).
- [26] D. H. Auston, *IEEE J. Quantum Electron.* **4**, 420 (1968).
- [27] P. L. Smith, *Proc. IEEE* **58**, 1342 (1970).

- [28] F. Krausz, T. Brabec, and C. Spielmann, *Opt. Lett.* **16**, 235 (1991).
- [29] S. R. Bolton, and M. R. Acton, *Phys. Rev. A* **6206** (2000).
- [30] B. Segard, S. Matton, and P. Glorieux, *Phys. Rev. A* **66** (2002).
- [31] G. L. Lippi, S. Barland, and F. Monsieur, *Phys. Rev. Lett.* **85**, 62 (2000).
- [32] X. Hachair, S. Barland, J. R. Tredicce, and G. L. Lippi, *Appl. Opt.* **44**, 4761 (2005).
- [33] E. Ott, C. Grebogi, and J. A. Yorke, *Phys. Rev. Lett.* **64**, 1196 (1990).
- [34] K. Pyragas, *Phys. Lett. A* **170**, 421 (1992).
- [35] T. Shinbrot, C. Grebogi, E. Ott, and J. A. Yorke, *Nature* **363**, 411 (1993).
- [36] P. Melby, J. Kaidel, N. Weber, and A. Hubler, *Phys. Rev. Lett.* **84**, 5991 (2000).
- [37] P. Melby, N. Weber, and A. Hubler, *Chaos* **15** (2005).
- [38] S. F. Elena, and R. Sanjuan, *Biosystems* **81**, 31 (2005).
- [39] V. P. Zhigulin, M. I. Rabinovich, R. Huerta, and H. D. I. Abarbanel, *Phys. Rev. E* **67** (2003).
- [40] V. P. Zhigulin, in *Dept. of Physics California Institute of Technology* (Dept. of Physics California Institute of Technology, USA, 2004).
- [41] J. M. Dudley, G. Genty, and S. Coen, *Rev. Mod. Phys.* **78**, 1135 (2006).
- [42] Q. R. Xing, W. L. Zhang, and K. M. Yoo, *Opt. Commun.* **119**, 113 (1995).

- [43] A. Apolonski, B. Povazay, A. Unterhuber, W. Drexler, W. J. Wadsworth, J. C. Knight, and P. S. Russell, *J. Opt. Soc. Am. B* **19**, 2165 (2002).
- [44] L. Petit, N. Carlie, K. Richardson, A. Humeau, S. Cherukulappurath, and G. Boudebs, *Opt. Lett.* **31**, 1495 (2006).
- [45] F. Smektala, C. Quemard, V. Couderc, and A. Barthelemy, *J. Non-Cryst. Solids* **274**, 232 (2000).
- [46] C. L. Zhan, D. Q. Zhang, D. B. Zhu, D. Y. Wang, Y. J. Li, D. H. Li, Z. Z. Lu, L. Z. Zhao, and Y. X. Nie, *J. Opt. Soc. Am. B* **19**, 369 (2002).
- [47] U. Keller, J. Weingarten, F. X. Kartner, D. Kopf, B. Braun, I. D. Jung, R. Fluck, C. Honninger, N. Matuschek, and J. A. derAu, *IEEE J. Sel. Top. Quant.* **2**, 435 (1996).
- [48] J. H. Lin, H. R. Chen, H. H. Hsu, M. D. Wei, K. H. Lin, and W. F. Hsieh, *Opt. Express* **16**, 16538 (2008).
- [49] Y. M. Liu, and P. R. Prucnal, *IEEE Photon. Technol. Lett.* **5**, 704 (1993).
- [50] C. Y. Wang, W. L. Zhang, and K. M. Yoo, *J. Opt. Soc. Am. B* **14**, 1881 (1997).
- [51] T. Tsang, *Opt. Lett.* **18**, 293 (1993).

Chapter 2 Experimentals

In this chapter, we used the ABCD law discussed in our previous work [1] to design and construct a ps-KLM Ti:sapphire laser operated at 1/3-degenerated cavity configuration ($G_1G_2 = 1/4$). We further introduced the measurement system used to observe the nonlinear behaviors including the self-starting mode-locking, pulse-train amplitude modulation and spatio-temporal instability.

2.1 Experimental construction for a symmetric KLM laser

The schematic experimental setup of the ps-KLM Ti:sapphire laser is shown in Fig. 2-1, which is a z-folded four-mirror cavity containing a 9-mm-long Brewster-cut Ti:sapphire rod (0.1% Ti^{3+} doped, FOM > 150) without any hard-aperturing slit and group-velocity compensation components. Without any GVD compensation, the single pass GVD for the 9 mm Ti:sapphire crystal is 576 fs^2 . A CW frequency doubled Nd:YVO₄ laser (Coherent, Verdi-V8) was used as the pumped source, and the pumped beam is focused by a plano-convex lens with focal length of 12.7 cm at the center of the laser rod. Two curved mirrors (M_1 and M_2) of 10-cm radius of curvature were tilted about 10.1° to compensate the astigmatism. The distance from M_1 to one end face of the laser rod is denoted as r_2 , and from the other end face to M_2 as r_1 . In order to operate the laser at 1/3-degenerated cavity configuration, we calculated the

parameters of the laser cavity by using the ABCD law. The distance of r_1 is 52.85 mm and r_2 is tunable from 52.80 mm to 52.89 mm, respectively. Two flat mirrors, a 98% high reflector M_3 and a 95% output coupler M_4 , were placed to form linear arms. The distance between M_1 and M_4 , as well as the distance between M_2 and M_3 , are 75 cm to form a near-symmetric cavity arrangement. The total length of the resonator is approximately 160 cm corresponding to 93 MHz of repetition rate.

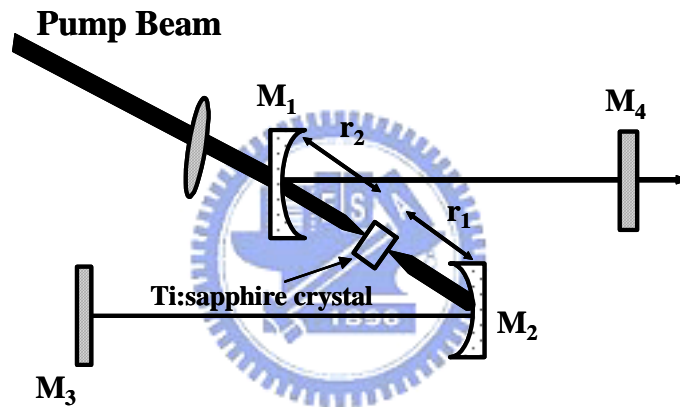


Fig. 2-1 The schematic experimental setup of the Kerr-lens mode-locking Ti:sapphire laser.

The lens, the laser rod, and the folding mirrors were mounted on precision translation stages with precision of $10\ \mu\text{m}$ to allow for fine adjustment of the resonator configuration and the overlap between pumped beam and cavity beam. The cold-cavity beam diameter at the center of the laser rod corresponds to $50\ \mu\text{m}$, which is larger than the pump one of $30\ \mu\text{m}$. By properly adjusting the cavity configuration we obtained KLM lasing including self-starting KLM [2, 3] that can be operated for a long

period of time. We measured the stable KLM pulse having the pulse width of about 3 ps. We observed the mode-locking regions occurred around the degenerated cavity configurations and this result have been reported in our previous work [1]. The mode-locking ranges are from 100 μm to 300 μm for the different degenerated cavity configurations. The self-starting mode-locking region ($\sim 30 \mu\text{m}$) occurred at the edge between the mode-locking region and CW region.

2.2 The measurement of self-starting Kerr-lens mode-locking

The self-starting was examined by blocking and unblocking the cavity beam to observe whether the laser will self-develop into the KLM state or not. We found the self-starting will always occur after the cavity beam is unblocked. The laser beam from M_3 was detected by a high-speed photodetector (Electro-Physics Technology ET-2000, with 300-ps rise time and noise equivalent power $10^{-13} \text{ W/Hz}^{1/2}$) and then connected to a 300-MHz digital oscilloscope (LeCroy 9450A) used to monitor and store the dynamic of laser for further analysis.

2.3 The observation of pulse-train amplitude modulation

We can operate the laser in the picosecond mode locking with central wavelength of 820 nm at pump power $P_p = 4 \text{ W}$ at the cavity length slightly longer than the 1/3-degenerate cavity configuration by properly tuning the mirror M_2 ($\sim 100 \mu\text{m}$ tuning

range) after a mechanical perturbation [1, 2]. When the curved mirror M_2 was translated slightly toward increasing the cavity length ($\sim 15 \mu\text{m}$), the sinusoidal amplitude modulation of the mode-locking pulse train was observed. We kept increasing the distance of r_1 , the pulse-train modulation presented intermittent modulation behaviors varying among period-2, period-3 and irregularity. By further increasing the distance of r_1 , self-starting mode-locking (within $30 \mu\text{m}$ tuning range) was observed, finally, the laser turned to CW output.

The laser beam from the high reflector M_3 was detected by two high-speed photodetectors with rise time $< 0.3 \text{ ns}$ and noise equivalent power $10^{-13} \text{ W/Hz}^{1/2}$. The output signals of photodetectors were sent to a LeCroy-9450A digital oscilloscope (300-MHz bandwidth) and a RF spectrum (HP 8560E) for monitoring the pulse sequence and the dynamics of Ti:sapphire laser.

2.4 The measurement of spatio-temporal instability

A CCD camera was used for observing the transverse pattern of the laser beam. The beam patterns observed for both the CW and picosecond KLM operations around the degenerate configuration are no longer pure fundamental Gaussian modes, which consist of several high-order Hermite–Gaussian modes with phase shifts relative to the fundamental one [1]. Figure 2-2 shows the beam pattern around the 1/3-degenerate

cavity configuration. We used two small-area detectors (0.006 mm^2) to measure intensities at different transversal positions of the pattern labeled A and B in Fig. 2-2.

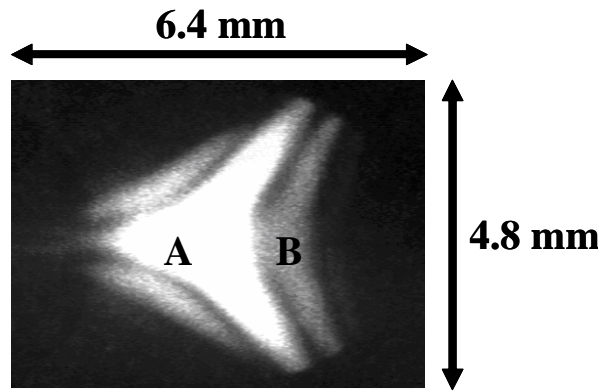


Fig. 2-2 The beam pattern around the 1/3-degenerate cavity configuration.



References

- [1] J. H. Lin, M. D. Wei, and W. F. Hsieh, *J. Opt. Soc. Am. B* **18**, 1069 (2001).
- [2] J. M. Shieh, F. Ganikhanov, K. H. Lin, W. F. Hsieh, and C. L. Pan, *J. Opt. Soc. Am. B* **12**, 945 (1995).
- [3] J. H. Lin, and W. F. Hsieh, *Opt. Commun.* **225**, 393 (2003).



Chapter 3 Numerical model

Many equations described the propagation of light in nonlinear media, either with or without a laser cavity, exhibit modulation instability. Examples are the nonlinear Schrödinger equation [1], the mode-locking master equation [2], and the laser Maxwell-Bloch equations [3]. Many of the above mentioned theories for the KLM lasers only considered the longitudinal modes but ignored the transverse modes. Experimentally, however, the nonlinear dynamics of a KLM laser depends on transverse modes around the degenerate cavity configurations [4]. In this chapter, we use the thin slab approximation [5] to simulate a pulse propagating in a laser cavity and present a simulation model based on the Fox-Li's approach including the optical Kerr effect in the rate equations [6] to simulate the dynamics of the nonlinear Kerr effect on the KLM laser operated around the 1/3-degenerate cavity configuration.

3.1 Thin slab approximation

Generally, we described how the optical radiation inside an optical cavity circulates repeatedly around the cavity, bouncing back and forth between the end mirrors, used only a plane-wave approximation but ignored the transverse spatial variation of the waves. To bring transverse variation into the discussion, let us consider only that portion of optical energy traveling in the $+z$ direction containing

within some short axial segment of length Δz within the cavity. We can think of the radiation in this segment as forming a short pulse or a thin “slab” of radiation as shown in Fig. 3-1, whose axial thickness Δz is small compared to the length of a typical cavity but still very large compared to an optical wavelength λ .

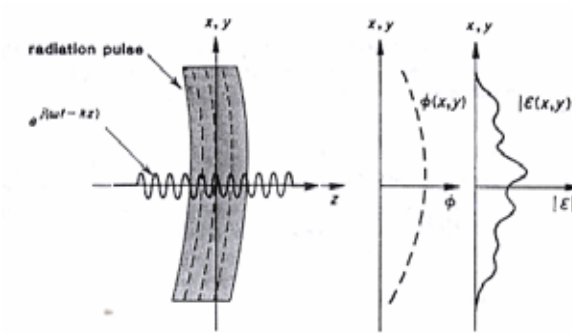


Fig. 3-1 A traveling pulse or “slab” of optical radiation propagating in the z direction.

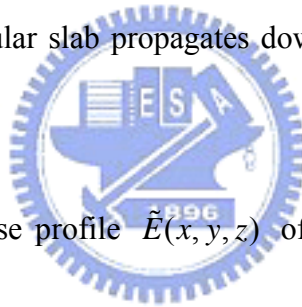
The time and space variation of the optical fields within such a circulating pulse or thin slab as it travels through the resonator can be written in the form

$$\begin{aligned} \mathcal{E}(x, y, z) &= \text{Re} \left[\tilde{E}(x, y, z) e^{j(\omega t - kz)} \right] \\ &= \text{Re} \left[\tilde{E}(x, y, z) e^{j(\omega t - kz) + j\phi(x, y, z)} \right] \end{aligned} \quad (3.1)$$

Here ω is the optical frequency and $k = \omega/c = 2\pi/\lambda$ the associated plane-wave propagation constant, and the complex phasor amplitude $\tilde{E}(x, y, z)$ describes the transverse amplitude and phase variation of the beam. By writing the fields in this fashion, we separate out the plane-wave aspects of the wave propagation as given by the $e^{j(\omega t - kz)}$ factor from the complex phasor amplitude $\tilde{E}(x, y, z)$. The transverse intensity profile of the beam within this particular phase or slab is the given by

$I(x, y, z) = |\tilde{E}(x, y, z)|^2$, where the transverse phase profile, or the shape of the optical wavefront is given by the transverse phase variation $\phi(x, y, z)$.

Although we write the phasor amplitude function $\tilde{E}(x, y, z)$ as a function of x , y and z , we will see later that the variation of this transverse beam profile with the axial or z coordinate is generally very slow compared to the e^{-jkz} variation that we separated out. The latter function goes through a complete $e^{\pm j2\pi}$ variation in just one optical wavelength. By contrast, the complex amplitude profile $\tilde{E}(x, y, z)$ will not change much if at all through the thickness of one “slab”; and it will also change only very slowly with distance as particular slab propagates down the resonator, or through free space outside a resonator.



If we follow the transverse profile $\tilde{E}(x, y, z)$ of any one such slab as it travels through one complete round trip around a laser cavity, we will definitely see the transverse field pattern in the slab change with distance as the slab propagates, diffracts, bounces off mirrors, and passes through laser rod, lenses and finite aperture. These changes in the transverse pattern $\tilde{E}(x, y, z)$ of the slab caused by propagation and diffraction are the primary effects that determine the transverse mode properties of optical beam and resonators. Further if we think a slab repeated round trips within a resonator, it can be regard as the pulse propagates through repeated sections of an iterated period optical system or lensguide as shown in Fig. 3-2. Hence we can find

the transverse mode patterns that are self-reproducing after each such round trip or periodic step by using a propagation integral

$$\tilde{E}^{(1)}(x, y) = e^{-jkp} \iint_{\text{input plane}} \tilde{K}(x, y, x_0, y_0) \tilde{E}^{(0)}(x_0, y_0) dx_0 dy_0, \quad (3.2)$$

where k is the propagation constant at optical frequency; p is the length of one round trip; and the integral is over the transverse coordinates at the input plane. The function \tilde{K} depends on the chosen reference plane is commonly called the propagation kernel or “propagator”, since the field $\tilde{E}^{(1)}(x, y)$ after one propagation step can be obtained from the initial field $\tilde{E}^{(0)}(x_0, y_0)$ through the operation of the linear kernel \tilde{K} . If the reference plane is chosen at an aperture and the only intervening element before the next aperture is simply free space, the function \tilde{K} will be simply Hygens’s integral for free space, with the integral being evaluated over the aperture at the input end of each round trip.

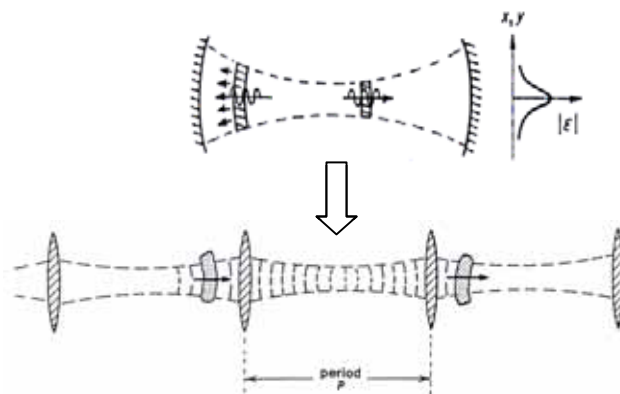


Fig. 3-2 The sketch of an iterated period optical (lensguide) system. Upper: Circulating pulses (“slab”) in an optical resonator. Bottom: Propagation through repeated round trips in an optical resonator is physically equivalent to propagation through repeated sections of an iterated period lensguide.

3.2 Huygen's integral and ABCD matrix

In the classical optics, we can use Huygens's integral to describe an optical field after a certain distance of diffraction. So we also can use Huygens's integral to describe laser beam in a real resonator. In Fig. 3-3, it is a sketch of one-dimension Huygens's integral, and it means that the optical field of plane Z_2 interferes with all of the point sources of plane Z_1 . In one-dimension condition, the Huygens's integral is

$$\tilde{u}_2(x_2) = \sqrt{\frac{j}{L\lambda}} \int_{-\infty}^{\infty} \tilde{u}_1(x_1) e^{-jk\rho(x_1, x_2)} dx_1, \quad (3.3)$$

where the $\tilde{u}_1(x_1)$ and $\tilde{u}_2(x_2)$ are respectively the wave functions on the Z_1 and Z_2 planes, k is the wave number and λ is the wavelength of laser field, $\rho(x_1, x_2)$ is the distance of the arbitrary position vectors on the Z_1 and Z_2 planes. Therefore we can define ρ as

$$\rho(x_1, x_2) = \sqrt{L^2 + (x_2 - x_1)^2} \approx L + \frac{(x_2 - x_1)^2}{2L}, \quad (3.4)$$

We can use Eqs. (3.3) and (3.4) to calculate the diffraction of optical field.

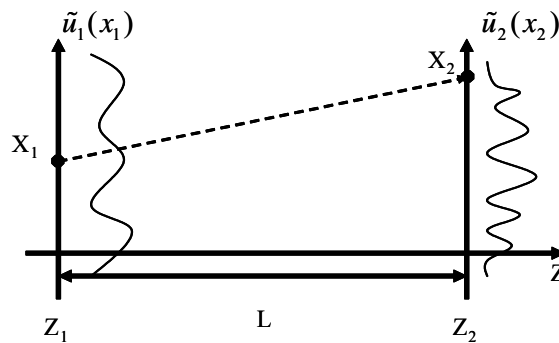


Fig. 3-3 The sketch of one-dimension Huygens's integral. L is the separation distance between planes of Z_1 and Z_2 , the $\tilde{u}_1(x_1)$ and $\tilde{u}_2(x_2)$ are the wave functions on these planes.

We usually use the ABCD matrix to present a paraxial system, such as laser resonator. If we substitute the elements of ABCD matrix to Huygens's integral, it will be very convenient to use. Now, we will find the relationship between $\rho(x_1, x_2)$ and ABCD matrix, and substitute to Huygens's integral. In Fig. 3-4, a paraxial optical system between the planes of Z_1 and Z_2 can be expressed as

$$\begin{bmatrix} x_1 \\ x'_1 \end{bmatrix} = \begin{bmatrix} A & B \\ C & D \end{bmatrix} \begin{bmatrix} x_2 \\ x'_2 \end{bmatrix}, \quad (3.5)$$

where the x and x' respectively represent the positions and slope of ray on the Z_1 and Z_2 planes. From Eq. (3.5), we can get the slope of each point as

$$\begin{aligned} x'_1 &= \frac{x_2 - Ax_1}{B} \\ x'_2 &= \frac{Dx_2 - x_1}{B} \end{aligned} \quad (3.6)$$



The input ray may be viewed as a ray coming from an object point P_1 located a distance R_1 behind the input plane, as shown in Fig. 3-4. Hence R_1 and R_2 is given by

$$\begin{aligned} \frac{R_1}{n_1} &\equiv \frac{x_1}{x'_1} = \frac{Bx'_1}{x_2 - Ax_1} \\ \frac{R_2}{n_2} &\equiv \frac{x_2}{x'_2} = \frac{Bx'_2}{Dx_2 - x_1} \end{aligned} \quad (3.7)$$

Fermat's principle says that "all rays connecting two conjugate points must have the same optical path length between two points." Therefore the ray path from P_1 to P_2 through x_1 and x_2 will equal to the ray path along the optical axis ($\overline{P_1P_2} = \overline{P_1x_1x_2P_2}$).

Both ray paths can be written as

$$\begin{aligned}
\overline{P_1 P_2} &= n_1 R_1 + L_0 - n_2 R_2 \\
\overline{P_1 x_1 x_2 P_2} &= n_1 (R_1^2 + x_1^2)^{1/2} + \rho(x_1, x_2) - n_2 (R_2^2 + x_2^2)^{1/2} . \\
&\approx n_1 (R_1^2 + \frac{x_1^2}{2R_1})^{1/2} + \rho(x_1, x_2) - n_2 (R_2^2 + \frac{x_2^2}{2R_2})^{1/2}
\end{aligned} \tag{3.8}$$

From Eq. (3.8) we can get

$$\rho(x_1, x_2) = L_0 + \frac{1}{2B} (Ax_1^2 - 2x_1 x_2 + Dx_2^2) . \tag{3.9}$$

By substituting Eq. (3.9) into Eq. (3.3), the Huygens's integral becomes

$$\tilde{u}_2(x_2) \sqrt{\frac{j}{B\lambda}} e^{-jkL_0} \int_{-\infty}^{\infty} \tilde{u}_1(x_1) e^{-j\frac{\pi}{B\lambda}(Ax_1^2 - 2x_1 x_2 + Dx_2^2)} dx_1 . \tag{3.10}$$

Therefore we have the relationship between element of ABCD matrix and the Huygens's integral.

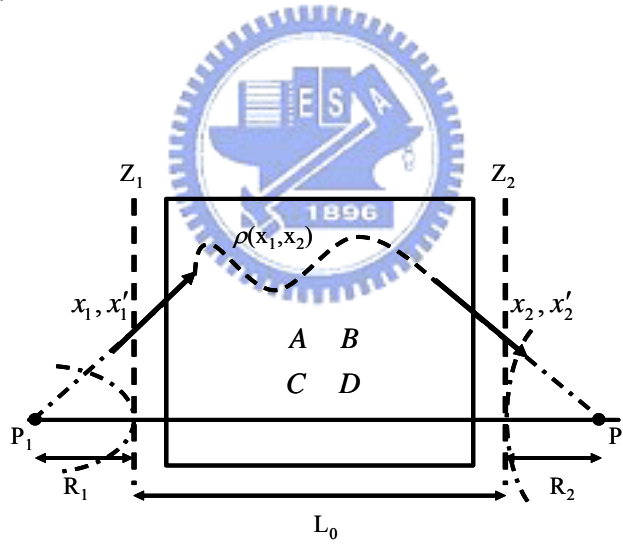


Fig. 3-4 The sketch of the optical ray through an ABCD paraxial system. The x and x' respectively represent position and slope of ray. P_1 is the conjugate point of P_2 .

3.3 Simulation model of the KLM laser

To simulate a KLM laser we constructed the equivalent four-mirror cavity system shown in Fig. 3-5. The cavity consists of two flat mirrors M_3 and M_4 , a 98% high

reflection end mirror M_3 and a 95% output coupler M_4 , and a pair of curved mirrors M_1 and M_2 with the same radii of curvature $R = 10$ cm. The laser rod also acting as a Kerr medium with the refractive index $n = 1.76$ and length l is placed between the curved mirrors. M_2 and M_4 form a linear arm with a distance of 75 cm and M_1 with M_3 at the same distance, respectively, in a near-symmetric arrangement. The distance r_2 from the curved mirror M_1 to one end surface of the Kerr medium is 53.625 mm and r_1 from the other end surface of Kerr medium to M_2 is tunable from 53.61 mm to 53.67 mm. The total length of the resonator L is approximately 160 cm. The laser cavity is operated at 1/3-degenerate cavity configuration. Here we assume that no dispersion exists in the system for our numerical model since there are no dispersion components in Fig. 3-5.

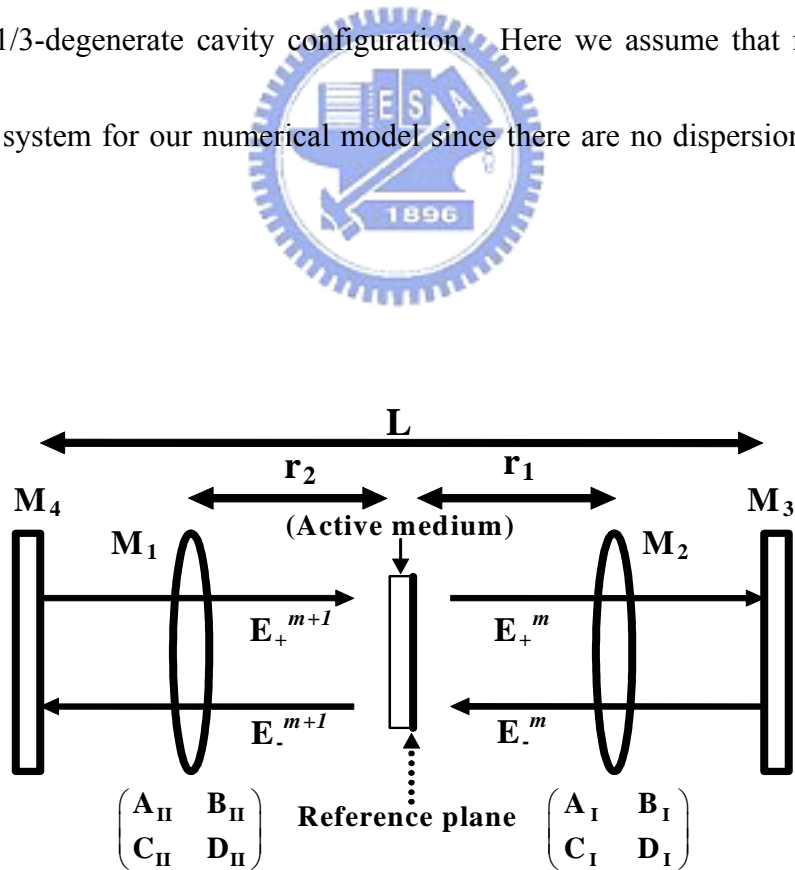


Fig. 3-5 Schematic of an equivalent four-mirror cavity configuration.

In nearly all of the situations of practical interest in mode-locked lasers, the time variation of mode-locked pulse is still slow compared with the dephasing time in the saturable absorbing medium; and the saturation behavior of the absorption will be essentially that of a simple homogeneous atomic transition. Moreover, most lasers used for technological applications belong to the so-called Class B lasers [5], which include all solid state, semiconductor, and CO₂ lasers. All these devices have in common the long lifetime of the excited state (relative to both the medium polarization lifetime and to the photon lifetime in the cavity). Basic rate equation model for a single longitudinal and transverse-mode Class B laser involves two equations describing rate of change of field and population inversion [7]. For Kerr-lens mode-locked lasers, however, the optical Kerr effect plays a role of fast saturable absorber. Hence, we can describe the nonlinear transition of an optical pulse through Kerr medium with sufficient accuracy using only a simple rate-equation approach, without going into more complex resonant-dipole or Rabi-flopping analyses [5].

Let the reference plane be end face I of the crystal. In a thin-slab approximation [5], which the axial thickness of a short pulse is small compared to the length of a typical cavity but still very large compared to an optical wavelength, we therefore numerically simulate this laser system by using Collin's integral [8] with round-trip

transmission matrix to calculate light field $E(r)$ under cylindrical symmetry, where r is the radial coordinate and the rate equations as described in our previous work [6],

$$E_{-}^{m}(r) = \frac{2\pi j}{B_1 \lambda} \int_0^a \exp[-jk(2d_1')] E_{+}^{m}(r') \exp[-(j\pi / B_1 \lambda) \times (A_1 r'^2 + D_1 r^2)] J_0(2\pi r r' / B_1 \lambda) r' dr' \quad (3.11)$$

with transmission matrix $\begin{bmatrix} A_1 & B_1 \\ C_1 & D_1 \end{bmatrix}$. Here $E_{+}^{m}(r)$ and $E_{-}^{m}(r)$ are the m -th propagating

optical field on the reference plane in Fig. 3-5 before and after Huygens diffraction, r'

and r are the corresponding radial coordinates, λ is the wavelength of laser, J_0 is the

Bessel function of zero order, d_1' is distance from end face I through the M_2 and the M_3 ;

and a is the aperture radius on the reference plane and it must be chosen large enough

with many times of the fundamental mode radius to ensure that the diffraction loss can

be neglected. In order to include the self-focusing effect in active medium, we

modified the equation to describe the light field passing through the gain medium by

adding the nonlinear phase shift, $\phi(r) = \frac{2\pi}{\lambda} n_2 I(r)$, which is caused by optical Kerr

effect, in the equation of field evolution:

$$E_{+}^{m+1} = E_{-}^{m} \exp\left(\frac{1}{2} g_m l - i\phi\right) + E_{spont}^m \quad (3.12)$$

Here E_{-}^{m} and E_{+}^{m} are the optical fields of the m th round trip just reaching and leaving

the laser rod; l is the length of gain medium, g_m is the gain coefficient, E_{spont}^m is the field

of spontaneous emission whose amplitude and phase are given by the spontaneous

decay term in Eq. (3.12) and a random generator, respectively; and n_2 is the nonlinear

refractive index. $I(r)$ is the intensity distribution of laser pulse calculated from the

optical field $E^m(r)$ using $I(r) = (1/2n\epsilon_0)|E^m(r)|^2$, where n is refractive index and ϵ_0 is permittivity of free space. Similar treatment is for the opposite direction propagation.

Note that because the length of gain medium is far smaller than the cavity length the gain distribution can be regarded as uniform distribution along the propagating direction.

If the thickness Δz of the pulse is far smaller than the length of gain medium, the pulse experienced the uniform gain.

The gain coefficient of the successive pass in the gain medium is related as

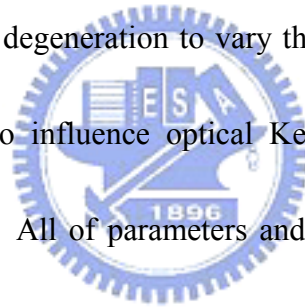
$$g_{m+1} = (1 - \gamma_a \Delta t) g_m + \frac{2\Delta t}{h\nu_p N_0 l} \left(\frac{P_p}{\pi w_p^2} e^{-\frac{2r^2}{w_p^2}} \right) (\sigma N_0 - g_m) - \frac{\gamma_a \Delta t}{|E_s|^2} |E_m|^2 g_m. \quad (3.13)$$

When we considered Eq. (3.12) without self-focusing effect ($n_2 = 0$), Eqs. (3.12) and (3.13) can use to model the laser dynamics with the beam-propagation dominant as cavity is far from degeneration but with interplay of beam propagation and gain dynamics as cavity is tuned toward degeneration [5]. However, if we considered the self-focusing effect, act as the so-called Kerr lens, it changes the electric field distribution and shrinks the spot size of the electric field to modify the gain profile and result in the KLM mode resonates more easily than the CW mode.

Here we used the spontaneous decay rate $\gamma_a = 3.125 \times 10^5 \text{ s}^{-1}$ [9], the total density $N_0 = 3.3 \times 10^{25} \text{ m}^{-3}$ [9], the length $l = 9 \text{ mm}$, the stimulated-emission cross section $\sigma = 3.0 \times 10^{-23} \text{ m}^2$ [10] and the saturation parameter $E_s = 1.05 \times 10^6 \text{ N/C}$ of the active medium [10]; and the round-trip time $\Delta t = 10.67 \text{ ns}$ that was determined by cavity

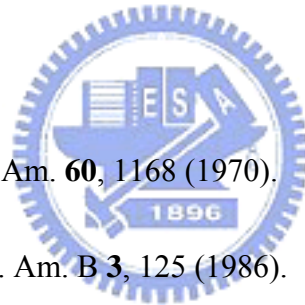
length, the photon energy of the pumping laser $h\nu_p = 1.53$ eV, and pumping beam radius $w_p = 15$ μm . We have omitted the dispersion of the active medium so that the gain is assumed to be real.

We calculated the laser output power by integrating the intensity distribution of laser pulse $I(r)$ with respect to the aperture radius a on the reference plane every roundtrip. The processes repeat in each roundtrip until reach convergence to continuous-wave steady state for CW laser output. In order to investigate the cavity-dependent instability, we set the initial values of $E(r)$ to zero, i.e., $E^1(r) = 0$, and changed r_1 across the point of degeneration to vary the optical field distribution in the gain medium corresponding to influence optical Kerr effect on laser dynamics for calculating the output power. All of parameters and variables used in program have been set double precision.



References

- [1] G. P. Agrawal, *Nonlinear Fiber Optics* (Academic, San Diego, Calif., 2001).
- [2] H. A. Haus, IEEE J. Sel. Top. Quant. **6**, 240 (2000).
- [3] H. Haken, *Synergetics* (Springer-Verlag, Berlin, 1978).
- [4] J. H. Lin, M. D. Wei, and W. F. Hsieh, J. Opt. Soc. Am. B **18**, 1069 (2001).
- [5] A. E. Siegman, *Lasers* (University Science Books, Mill Valley, California, 1986).
- [6] C. H. Chen, M. D. Wei, and W. F. Hsieh, J. Opt. Soc. Am. B **18**, 1076 (2001).
- [7] X. Hachair, S. Barland, J. R. Tredicce, and G. L. Lippi, Appl. Optics. **44**, 4761 (2005).
- [8] S. A. Collins, J. Opt. Soc. Am. **60**, 1168 (1970).
- [9] P. F. Moulton, J. Opt. Soc. Am. B **3**, 125 (1986).
- [10] J. F. Pinto, L. Esterowitz, G. H. Rosenblatt, M. Kokta, and D. Peressini, IEEE J. Quantum Electron. **30**, 2612 (1994).



Chapter 4 Results and Discussion

In this chapter we discussed our experimental and simulated results. We observed the self-starting Kerr-lens mode-locked without external modulation and feedback control [1]. In order to confirm the state of the transition from free-running spiking to mode-locking, the correlation function and the correlation dimension based on the Grassberger-Procaccia analysis (GPA) [2] were applied. The non-integer correlation dimension and autocorrelation show it is a chaotic state.

We also observed pulse-train modulation in a picosecond self-mode-locked Ti:sapphire laser with pump-power dependence when it was operated around the degenerate cavity configuration [3]. The envelope of periodic amplitude modulation splits into two or three clusters with enhanced modulation depth as increasing the optical pumping power and then the amplitude modulation eventually becomes disordered at higher pump power. Owing to the optical Kerr effect in a picosecond self-mode-locked Ti:sapphire laser is smaller than in a femtosecond self-mode-locked Ti:sapphire laser the amplitude modulation may be supported by exciting two sets of non-degenerate longitudinally mode-locked supermodes due to spatially inhomogeneous gain modulation in the Ti:sapphire crystal.

We numerically studied suppressing chaos to reach completely mode-locking in a self-starting Kerr-lens mode-locked (KLM) laser [4]. By using the Collins integral and rate equations with and without the self-focusing effect, we found without the self-focusing effect typical laser output and the feature of a power dip agrees with the observation of experiment [5] for all calculated cavity configurations around the degeneracy at various pump powers. However, by including the self-focusing effect, the time evolution of the pulse-train envelope presents various states including continuous wave or periodic state and instability such as period, period-2, and irregular states. The simulated self-starting KLM output, which possesses transient irregularity before reaching a constant amplitude output, occurs between the instability and continuous wave regions. The self-focusing acts as a slow-varying control parameter that suppresses the transient chaos to reach a stable mode-locking state in a self-starting Kerr-lens mode-locked Ti:sapphire laser without external modulation and feedback control. The self-adaptation occurs at the boundary between the chaotic and continuous output regions in which the laser system begins with a transient chaotic state, and then evolves with reducing dimension into the stable ML state. Furthermore, the different runs of the simulated self-starting from the spontaneous emission reveal the buildup time of mode-locking not only is sensitive to the initial condition but also presents the distribution with exponential decay. Its return map presents chaotic state

with a strange attractor in the initial stage. It transits to the quasi-periodic state and finally converges to a fixed point with time evolution.

4.1 Nonlinear dynamics analysis of Self-starting KLM laser

Figure 4-1 shows the typical evolving output of the self-starting KLM laser developed from spontaneous noise under 5W CW pumping. Apparently, the laser first oscillated with free running spiking once the cavity path was unblocked. It then evolved into stable KLM operation with a pulse width of 3 ps. To verify the determinism of the data, the correlation function and the correlation dimension proposed by the Grassberger-Procaccia analysis (GPA) [2] were applied.

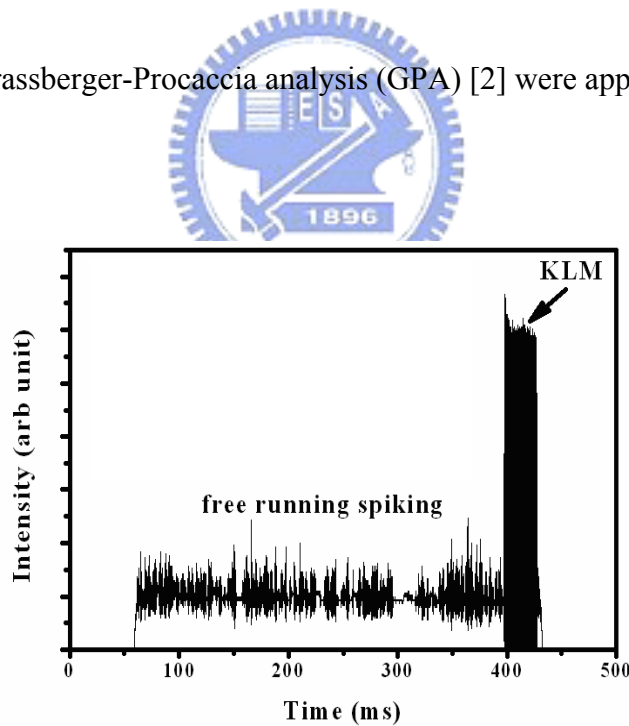
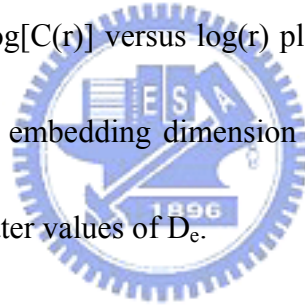


Fig. 4-1 The output clusters of the self-starting pulse train on the oscilloscope with 5 W pumped. The CW laser oscillated with free running spiking when the cavity path was unblocked and then suddenly broke into KLM operation.

To do the GPA, the time embedding technique is required to construct the trajectory in the D_e embedding dimensions with a vector y_i . The number of pairs of points with a separation distance less than some value r is estimated by

$$C(r) = \lim_{N \rightarrow \infty} \frac{2}{(N - D_e + 1)(N - D_e)} \sum_i^{(N - D_e + 1)} \sum_{j > i}^{(N - D_e + 1)} H(r - (y_i - y_j)), \quad (4.1)$$

where y_i and y_j are the coordinates of the i th and j th vectors of total N data, and H is the Heaviside function, which is defined as $H(u) = 1$ if $u > 0$, but zero otherwise. The distance r can be simply a Euclidean norm and represents the size of measurement window. Because $C(r)$ could vary as $C(r) \approx r^d$, where d is the dimension of the attractor, by the slope of the $\log[C(r)]$ versus $\log(r)$ plot it is possible to determine d if we have the correct minimum embedding dimension whose slope would convert to a value despite choosing the greater values of D_e .



The measured data in the experiment represent a discrete time sequence of laser outputs $x(t)$, recorded by an oscilloscope with a sampling interval of τ , and represented by $x(\tau_0 + n\tau)$ or x_n . For the nonlinear dynamic analysis, we have reported detailed bifurcation diagrams and verified the determinism of the chaotic state in the soft-aperture KLM [6]. Here we used 30,000 data points of transient irregularity with 0.01 ms sampling time before the complete KLM. Figure 4-2 shows the slope of $\log[C(r)]$ versus $\log(r)$ for the embedding $D_e = 2$ to 12. When the length scales are smaller or equal to the noise strength, the noise will cause fuzziness so that we would

recognize only $C(r) \approx r^d$ for $r > r_{\text{noise}}$. This value d increases until it reaches a constant value as the embedding dimension D_e is large enough to accommodate the attractor. A plateau can be seen within proper length scale in Fig. 4-2 with a finite and non-integer value of $d = 2.11 \pm 0.08$, indicating the transient irregularity is chaotic. The chaotic characteristic can be confirmed further by observing the revivals of the autocorrelation function for a long delay time, as shown in the inset of Fig. 4-2.

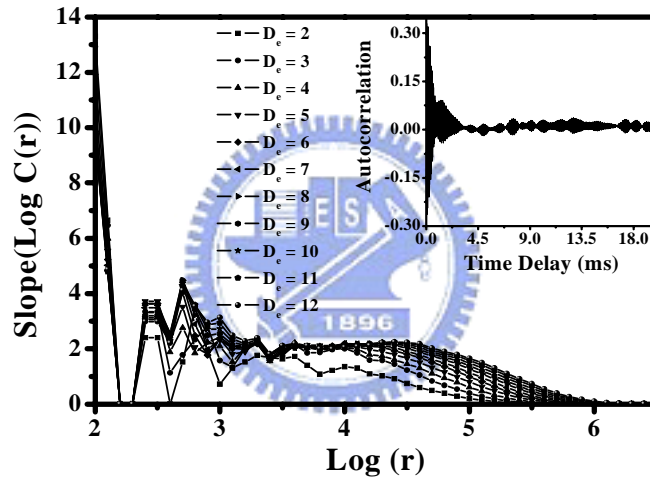


Fig. 4-2 The calculated $\log [C(r)]/\log(r)$ versus $\log(r)$ with embedding dimension D_e from 2 to 12 by the GPA. The inset is the damped autocorrelation that reveals a chaotic characteristic.

The laser instabilities, e.g., the instabilities of single mode [7] and multimode [8, 9] lasers and transverse instabilities [10], are generally described by Maxwell-Bloch equations. However, since the Ti:sapphire laser is a class B laser, the polarization relaxation rate is faster than those of field and population, and the Maxwell-Bloch equations are reduced to the rate equation. Furthermore, in the passive mode-locked

laser, the OKE can be exploited to simulate the fast saturable absorber behavior and the rate-equation approach can describe sufficiently the transmission of an optical pulse through such a fast saturable absorber without using more complex resonant-dipole or Rabi-flopping analyses [11]. For comparison with the experimental observation, and to ascertain that the chaotic characteristic is a result of the self-focusing effect, we numerically simulated this laser system by using Collin's integral [12] with round-trip transmission matrix to calculate the light field $E(r)$ under cylindrical symmetry, where r is for the corresponding radial coordinates and the rate equations are as described in our previous work [13].

Without considering OKE ($n_2 = 0$), typical laser output begins with a relaxation oscillation and then a stable output in all the stable cavity configurations [13]. Let $n_2 = 3 \times 10^{-20} \text{ m}^2\text{W}^{-1}$ and pulsewidth $\tau_p = 3 \text{ ps}$; the laser output states versus the tuning range are shown in the inset of Fig. 4-3. The stable laser output after the relaxation oscillation can be seen in the CW regions. However, instability output can be seen as the cavity configuration tuned close to the degenerate cavity configurations, set here around 1/3-transverse degeneracy, in which the transverse modes with mode numbers $m+n = 3N$ have the same frequency as the fundamental mode, where N is an integer.

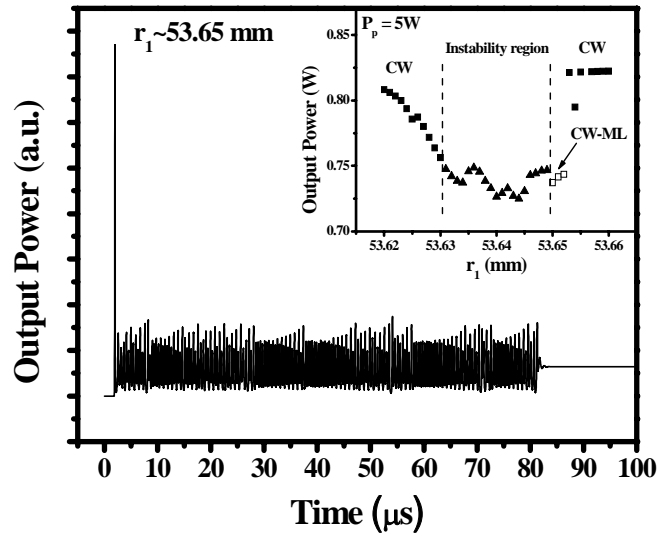


Fig. 4-3 The laser output power around the degenerate cavity configuration. A large fluctuation is similar to the situation of the transient irregular spiking before the KLM as shown in Fig.1. The inset is the lasing states versus cavity tuning, where r_1 is the distance between the curved mirror M_2 and the end face of the laser crystal.



The laser is situated either quasi-periodic or chaotic between $r_1 = 53.63$ and 53.65 mm (solid triangles), e.g., they are completely chaotic at $r_1 = 53.64$ mm and operated at CW state (solid squares) after transient oscillation for $r_1 < 53.63$ mm and $r_1 > 53.655$ mm. It is worth noting that the simulated SSKLM output as shown in Fig. 4-3, which is operated at CW-ML state (open squares), is similar to the experimental one (see Fig. 4-1), which possesses transient irregularity before reaching a constant output at $r_1 = 53.65$ mm. However, we cannot determine directly whether the constant output is completely KLM or CW output, due to lack of temporal information within a round trip time. By analyzing the simulated data in this case, we also obtained a similar decaying correlation function as the results of analyzing the experimental data in Fig. 4-3, with

correlation dimension of 1.67 ± 0.15 . Furthermore, the simulated result shows that the CW-ML occurred at the edge of a power dip around a degenerate cavity configuration, and it also agrees with our experimental reports [5].

To investigate the evolution of the SSKLM laser from the transient chaos into complete mode locking, we divided the 30,000 transient irregularities of the experimental data points into five parts with 10,000 data points per section, but overlapping 5,000 data points with the successive sections to calculate the evolving of the correlation dimension. However, the pulse peak detection based on Bolton et al. [14] must be used for the data of the complete KLM pulses. We therefore recorded separately the successive mode-locking pulses during the complete KLM. We acquired each mode-locking pulse containing 5 to 6 points and a total of 3,500 pulses for this calculation. Each data point represents an accumulation over approximately 2 ns. The maximum value of the voltage on the oscilloscope, with 8-bit flash, was read as approximately 2 V for our measured pulse train [6]. Shown in Fig. 4-4(a), the correlation dimension initially is a non-integer ($d = 2.56 \pm 0.17$), and then declines gradually to an integer dimension ($d = 1$). Finally, it evolves to a periodic complete KLM state corresponding $d = 0$. Correspondingly, for the simulation results, the correlation dimension calculating from the data of Fig. 4-3 evolves similarly from 1.88 to 1, then to $d = 0$. Furthermore, the characteristics of the phase space can be derived

by a plot, named “return map” obtained from the time series that is the observed output of the dynamical system [15]. A return map of the simulated SSKLM result is shown in Fig. 4(b). It presents a strange attractor in the initial stage. With time evolution, the chaotic state transits to the quasi-periodic (metastable) state corresponding to $d = 1$ and then converges to a fixed point ($d = 0$).

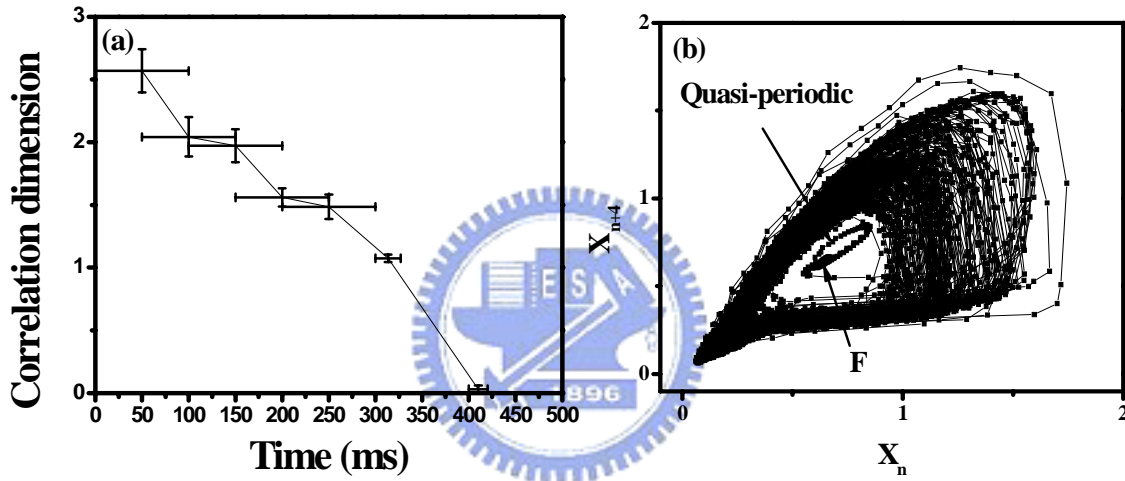


Fig. 4-4 The time evolution of the correlation dimension of the observed (a) and the return map of simulated output power (b). F: fixed point.

Lasers are typical systems in which the “slaving principle” applies, as Haken [16] has elegantly explained. In general, any kind of laser can be described by means of a set of coupled non-linear differential equations involving the first-order time derivatives that can be represented as $\frac{d\vec{x}}{dt} = F_{\vec{\mu}}(\vec{x}, t)$. The time-dependence vector $\vec{x} = (x_1, \dots, x_n)$ represents the n dynamical variables describing the laser system, so that its evolution defines a trajectory or orbit of the system in the phase space defined by these variables,

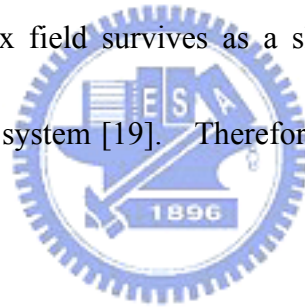
and the vector field F_{ii} describes the nonlinear coupling between the dynamical variables in a given kind of laser. Generally, F_{ii} depend on several control parameters designated by a vector $\vec{\mu} = (\mu_1, \dots, \mu_p)$ that characterizes each specific set of experimental conditions. If the control parameter μ_j is much larger than the remaining ones, the influenced variable x_j rapidly “loses” the memory of its history (i.e., of the values reached at preceding times); in such a way, it adapts rapidly to the instantaneous values reached by the remaining variables approximately proportional to μ_j . Therefore, the slowly evolving variables completely determine the evolution of the physical system. The self-focusing effect may play a role of slowly controlling the parameter to the studied laser system, and the slaving principle can be applied to describe the observed time evolving correlation dimension and the transient return map from the chaotic state to ML state.



In our previous reports, the laser dynamics are dependent on laser cavity configuration. The transverse-mode pattern is consisting of high-order transverse modes in a degenerate cavity configuration [5, 17]. Owing to the superposition of high-order modes, the transverse mode could be self-adjusted to match the pumping profile for extracting maximal pumped gain in cavity. The laser dynamics shows existence of temporal or spatial temporal instabilities when the nonlinear effects were in existence around the degenerate cavity configurations [17]. The Kerr-lens

mode-locking in a Ti:sapphire laser is dependent on the cavity configuration, no matter whether it is operated in picosecond or femtosecond pulse [5]. The ML region, varying the distance between the mirror and the crystal, is $\sim 300 \mu\text{m}$ including the self-starting ML in smaller region $\sim 30\mu\text{m}$. When the mirror was tuned within $30 \mu\text{m}$ range, the laser parameters, such as the beam waist of the cold cavity, cavity loss etc., would be unchanged but change in the relative Gouy phases of the transverse modes [18]. The pulse energy is fixed but waist is not, in a stable mode-locked laser.

It is known that, far from the threshold of continuous (supercritical) instability, only the phase of the complex field survives as a slow degree of freedom, since it describes the symmetry of the system [19]. Therefore, the nonlinear phase due to the nonlinear Kerr coefficient



$$\gamma = n_2 / (n_0^3 A_{eff}) \quad (4.2)$$

may act as the slowly varying control parameter [20]. Here n_0 is the linear refractive index and A_{eff} is the effective area in the Kerr medium [21]. Because the optical field originates from the spontaneous emission whose spot size is approximately corresponding to the spot size of the pumped beam, which is smaller than the spot size of a cold cavity, the initial values of $1/A_{eff}$ are almost constant, which is equal to $1.4 \times 10^{11} \text{ m}^{-2}$ as shown by a dash line in Fig. 4-5. $1/A_{eff}$ calculated at $N = 10,000$ round trips is equal to $3 \times 10^{11} \text{ m}^{-2}$ at CW-ML state, which is sandwiched between instability

and CW regions in the inset of Fig. 4-3. By plotting the probability of finding $1/A_{eff}$ after 10,000 round trips as a function of γ in a wide cavity tuning range of 70 μm in Fig. 4-5, we found γ does adapt to the edge of chaos that has the highest probability.

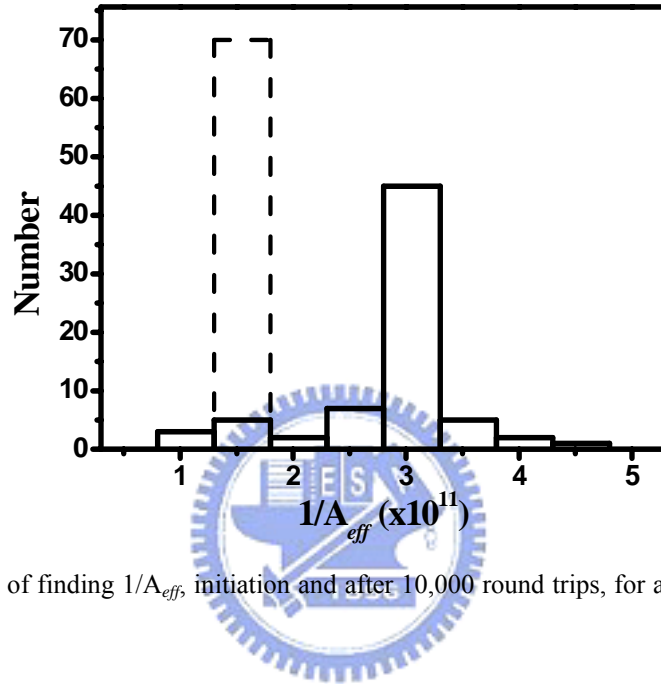


Fig. 4-5 Distribution of finding $1/A_{eff}$, initiation and after 10,000 round trips, for a cavity tuning range of 70 μm .

4.2 Pulse train amplitude modulation

The pumping threshold of mode-locking is about 3 W. We can operate the laser in the picosecond mode locking with central wavelength of 820 nm at pump power $P_p = 4$ W at the cavity length slightly longer than the 1/3-degenerate cavity configuration by properly tuning the mirror M_2 ($\sim 100 \mu\text{m}$ tuning range) after a mechanical perturbation [5, 22]. When the curved mirror M_2 was translated slightly toward increasing the cavity length ($\sim 15 \mu\text{m}$), the sinusoidal amplitude modulation of the mode-locking pulse

train was observed as shown in Fig. 4-6(a). We kept increasing the distance of r_1 , the pulse-train modulation presented intermittent modulation behaviors varying among Fig. 4-6(b)-(d). By further increasing the distance of r_1 , self-starting mode-locking (within 30 m tuning range) was observed, finally, the laser turned to CW output.

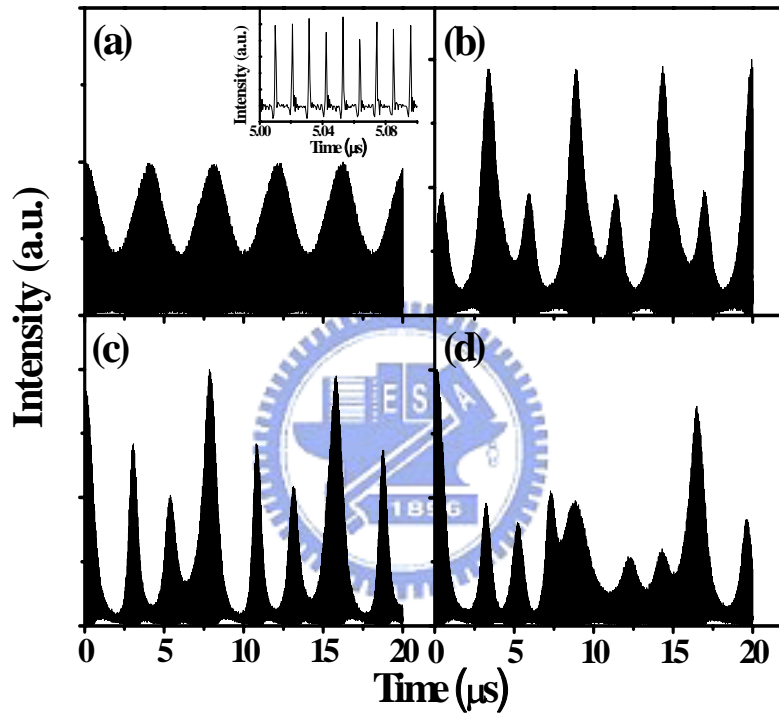


Fig. 4-6 Power-dependent mode-locked pulse-train modulations. (a) Periodic modulation pulse-train with 4 W pump power; (b) The modulation envelope splits into two clusters with 4.2 W pump power; (c) The modulation envelope splits into three clusters with 4.5 W pump power; and (d) irregular modulation of pulse-train with 5 W pump power. Inset: mode-locked pulses inside the modulation envelope of Fig. 4-6 (a).

Besides, by increasing the pump power from 4 W to 5 W, we observed the pulse-train modulation progressively changed from the sinusoidal amplitude modulation state of Fig. 4-6(a) to Fig. 4-6(b)-(d). The modulation rate was estimated

approximately at 250 kHz and the modulation depth was about 50 percent in Fig. 4-6(a). As the pump power is increased, the modulation rate increases and each of the self Q-switch pulses progressively splits into period-two at $P_p = 4.2$ W, period-three at $P_p = 4.5$ W, and then becomes irregular at $P_p = 5$ W as shown in Fig. 4-6(b)–(d), respectively. We also observed there is a period-doubling route to chaos with increasing pump power. Notice that the mode-locked pulses within the modulation envelope as in the inset of Fig. 4-6(a) show that each of the individual mode-locked pulses does not split due to the high-order solitons [23, 24] in any cases of the above-mentioned pulse-train modulation, because the optical Kerr effect in picosecond Ti:sapphire laser may not be strong enough to induce pulse-splitting behavior [25]. Furthermore, the filtering mechanism from the loss difference [24, 25] need not be considered because the gain band width of the picosecond pulses is much smaller than the band width of mirror reflectance.

The extended power spectra of different modulation states of Fig. 4-6 look alike shown as in the inset of Fig 4-7(a) with the repetition rate remaining ~ 93.3 MHz. We then further expanded the power spectra of the pulse-train modulations at the central frequency 93.3 MHz and shown in Fig. 4-7(a)–(d). The beat frequency located beside the central frequency corresponds to the pulse-train modulation frequency. The frequency of periodic modulation is 244 kHz, which agrees with the estimated 250 kHz from oscilloscope trace in Fig. 4-6(a). As pumping increases, the modulation

frequency increases first to become 366 kHz with subharmonic at 188 kHz (see Fig. 4-7(b)) in the period-two modulation as the time trace in Fig. 4-6(b); and then to become 366 kHz with period-three beating of 122 kHz and 244 kHz as shown in Fig. 4-7(c). The modulation turns to irregular with no dominant peaks in Fig. 4-7(d) if further increasing the pump power.

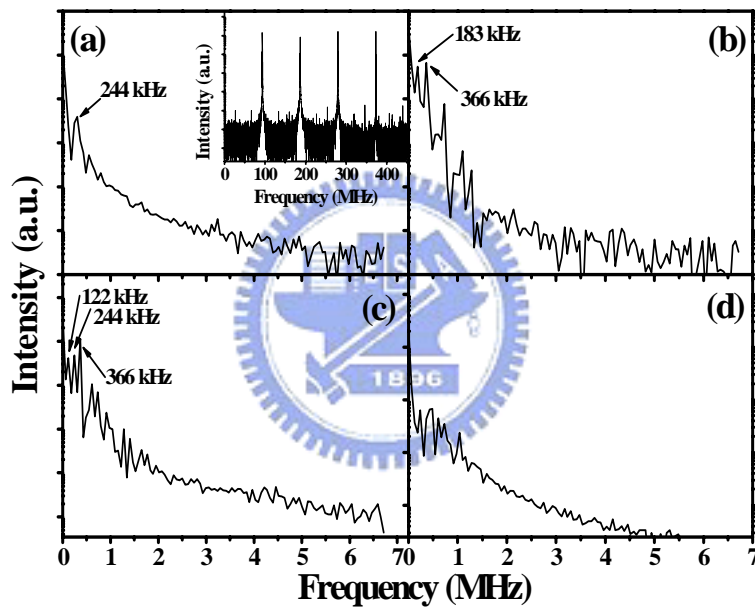


Fig. 4-7 The expanded power spectra of different modulation state of Fig. 4-6 at the central frequency 93.3 MHz. Inset: the power spectrum in coarse scale to the repetition frequency of 93.3 MHz.

Because the upper-state lifetime of Ti:sapphire crystal is $3.2 \mu\text{s}$ and the laser threshold is about 3 W, we estimated the relaxation oscillation frequency to be about 229 kHz [21]. A detailed theoretical study of self-Q switching was performed by Haus [26]. The frequency that corresponds to the several-microsecond period of

self-Q-switching is close to the relaxation oscillation frequency, which can be explained by the nonlinear interaction between the population inversion in the gain medium and the optical-field intensity in the cavity. However, since M_2 is translated only by $15\ \mu\text{m}$ and the parameters, such as the beam waist of the cold cavity, cavity loss etc., are almost unchanged, the modulation behavior is not induced by cavity loss. Therefore, the modulation mechanism should not be only Q-switching. In addition, in a femtosecond Ti:sapphire laser, soliton-like pulse shaping is dominant by balancing the self-phase modulation (SPM) in the Ti:sapphire rod and the net negative group velocity dispersion (GVD) provided by prism pair or chirped mirrors. Because GVD compensation prisms are absent in our picosecond mode-locked Ti:sapphire, the laser pulses would not form solitons. Therefore, the modulation mechanism should be different from that of Tsang's paper [23]. Also, unlike Liu's [27] or Xing's [28] resonator setups, our picosecond mode-locked laser is based on the soft-aperture effect in the Ti:sapphire crystal instead of using a hard aperture.

However, in an axially pumped laser, especially for the soft-aperture KLM laser with the pump size less than the cavity beam size, it is easy to excite the higher-order transverse modes to extract more stored energy from the gain medium when the laser is operated in the degenerate cavity [5]. The slow amplitude modulation of mode-locked pulse train may be due to the transverse modes interaction. For verification, we have

used two small-area detectors to measure intensities at different transversal positions of the pattern labeled A and B of Fig. 2-2. Fig. 4-8 shows the intensities of the laser simultaneously detected at two transversal positions. Not only both of the period-two pulse trains but also inverse evolution was observed at positions A and B, revealing that the transverse pattern is non-stationary and exhibits a spatial-temporal instability. Therefore, the slow pulse-train amplitude modulation should be dominated by transverse modes interaction rather than longitudinal modes interaction.

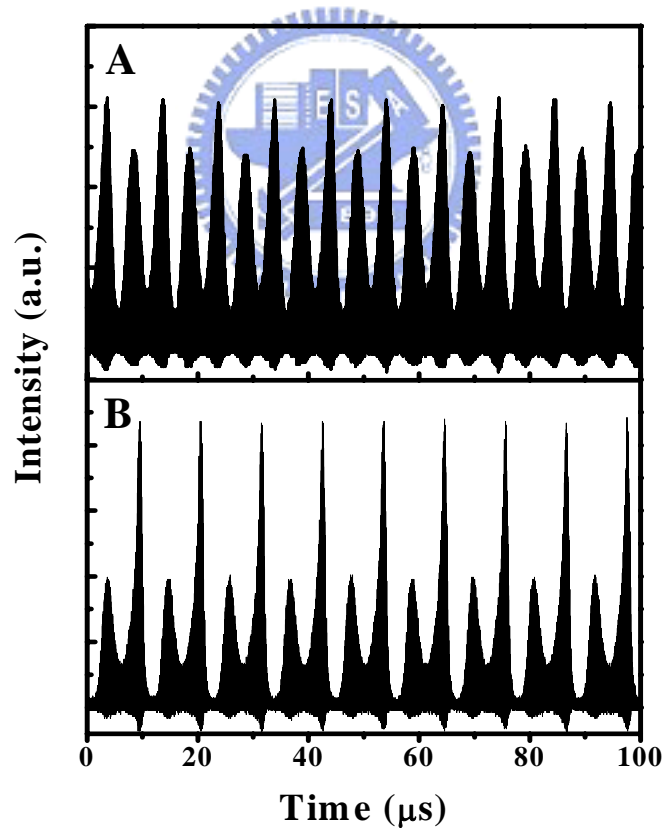


Fig. 4-8 The simultaneous intensities of the laser at two transversal positions labeled A and B in the inset of Fig. 2-2.

Typically, if only one spatial mode of the electromagnetic field is excited in the laser, the interesting instabilities are temporal [29, 30]. Nevertheless, under some circumstances, parameters can be adjusted so that more spatial modes come into play and spatio-temporal instabilities [31] also appear. Lugiato et al. expressed the Maxwell–Bloch equations in terms of modal amplitudes by using a suitably cylindrically symmetric empty-cavity-mode expansion [32, 33]. They presented a variety of spatiotemporal instabilities, including chaos and cooperative frequency locking, which occur under uniform and low-power pumped, by tuning the mode spacing. They were able to do this because the Laguerre–Gaussian modes are a set of good bases only when the uniform-field limit is applied for a so-called good cavity with small gain. Thus, their results are valid only for a laser in which the pump size is larger than the minimum cavity beam waist [34]. However, in axial-continuously pumped lasers, gain saturation provides an inherently nonlinear effect and when the pump size is smaller than the waist of the cold cavity, peculiar lasing behaviors [18, 35-38] have been observed in an end-pumped solid-state laser near the degenerate configurations that correspond to the low-order resonance. At these degenerate cavity configurations, because of the superposition of high order degenerate modes, the transverse mode pattern can be self-adjusted to match the pumping profile for extracting maximal pumped gain in the cavity, a supermode or superposition of phase-locked

degenerate transverse modes can be formed with relatively low lasing threshold. Beam waist shrinkage [37] and operation of a stable CW bottle beam [18, 38] were observed around the degenerate cavities. As in our previous report [13], under tightly axially pumped, the laser would possess spatio-temporally instability if the cavity length is detuned away longer than that of the degenerates. We believe that the detuning of the cavity from the degenerates may result in excitation of another supermode due to spatially inhomogeneous gain. This new supermode is no longer degenerate with the fundamental mode but has a frequency shift corresponding to the Guoy phase. We estimated the length detuning length of the cavity is $\sim 15 \mu\text{m}$. Therefore, we believe that the amplitude modulation may result from competition of these two sets of longitudinally mode-locked supermodes, which no longer can be phase locked by gain saturation.

Because in the Kerr-lens mode-locked laser, the optical Kerr effect can be exploited to simulate the fast saturable absorber behavior, and the rate-equation approach can describe sufficiently the transmission of an optical pulse through such a fast saturable absorber [11, 13]. Here, we simulated the slow amplitude modulation behavior of this picosecond Kerr-lens Ti:sapphire laser based on the Fox-Li's approach, including the self-focusing effect and using the Collin's integral with the rate equations [13].

Fig. 4-9 shows the simulated output power with changing the effective pump power P_p from 4 W to 5 W with and without nonlinear refractive index n_2 . By setting the nonlinear index $n_2 = 0$, we found that evolution of laser output is always continuous after relaxation oscillation, as shown in the Fig. 4-9(a), for the cavity was set for $r_1 = 53.620$ mm to 53.645 mm and P_p from 4 W to 5 W. However, let $n_2 = 3 \times 10^{-20} \text{ m}^2\text{W}^{-1}$, pulsewidth $\tau_p = 3$ ps and $P_p = 4\text{W}$, the laser output power versus r_1 (Fig. 4-9(b)) shows the region of various states such as CW output (solid squares), period modulation (open circles) and irregular modulation (solid triangles), etc. When r_1 is smaller than 53.629 mm the laser output presents CW output (solid squares). However, we cannot determine directly whether the constant output is completely KLM or CW output due to lack of temporal information within a roundtrip time and mechanical perturbation term. The simulated time sequence of output power in the unit of roundtrip time corresponds to the envelope amplitude in Fig. 4-6. The period modulation state (open circles), whose envelope is similar to Fig. 4-6(a), is located between $r_1 = 53.630$ mm and 53.631 mm; the period-2 modulation state (open triangles) is at $53.633 \text{ mm} < r_1 < 53.637 \text{ mm}$; and the irregular modulation state (solid triangles) is at $r_1 = 53.632 \text{ mm}$ and $53.638 \text{ mm} < r_1 < 53.641 \text{ mm}$; and the laser output may become CW or KLM (open squares) at $r_1 > 53.642 \text{ mm}$. Although due to lack of temporal information within a roundtrip time, we cannot determine directly whether the constant output is self-starting KLM or CW

output, we would expect observing self-starting KLM then CW output as known from the experimental observation. The simulated pulse-train modulation with varying r_1 was similar to our observation and the character of the output power dip was similar to the Ref. 5.

At the position deviating from the degeneration, $r_1 = 53.635$ mm, the pulse-train amplitude modulation changed from period-two to irregular for pump power being 4W and 4.5W respectively, as shown in Figs. 4-9(c) and (d), which are similar to Figs. 4-6(b) and (d). The amplitude modulation frequency is about 750 kHz in Fig. 4-9(c).

Owing to the fact that the pump power in the simulation may be higher than the actual one, the amplitude modulation frequency of the simulation is larger than the measured modulation frequency. Furthermore, in our previous reports [5, 17], the transverse mode pattern consisted of high order transverse modes around the degenerate cavity configuration. Because of the superposition of high order modes, the transverse mode could be self-adjusted to match the pumping profile for extracting maximal pumped gain in the cavity. The optical Kerr effect played a role that enhanced beam waist shrinkage and supermodes generation as the small pump spot size. Therefore, the subharmonic amplitude modulation may result from competition of these sets of longitudinally mode-locked supermodes, which no longer can be phase locked by gain saturation.

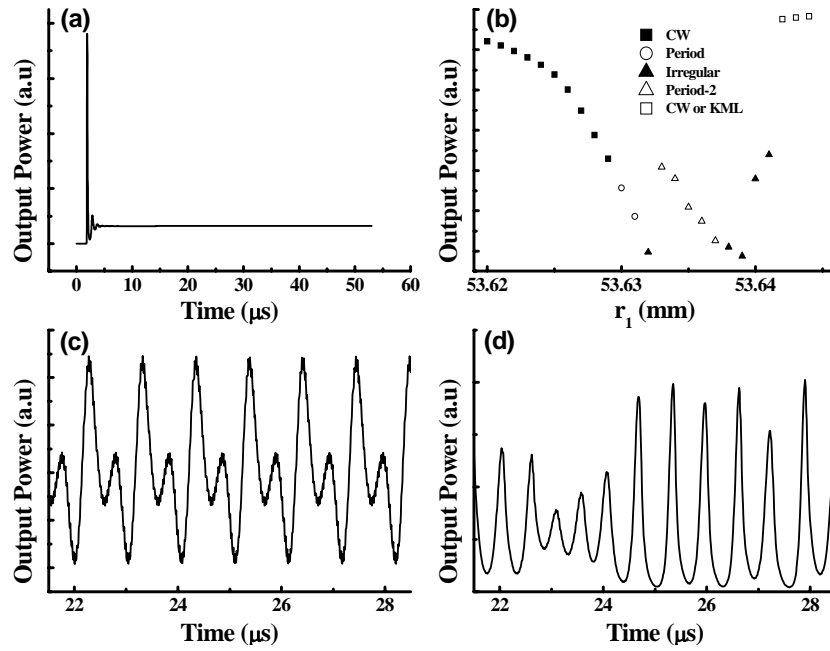


Fig. 4-9. The simulated evolution of output power with changing pump power from 4 W to 5 W with and without Kerr effect. (a) It always shows continuous output after relaxation oscillation over the calculated cavity configurations without Kerr effect ($n_2 = 0$); with Kerr effect on $n_2 = 3 \times 10^{-20} \text{ m}^2 \text{ W}^{-1}$, (b) the cavity tuning region of various dynamic behaviors (e.g., period, period-2, irregular, etc., labeled in the inset) around the degenerated configuration at $P_p = 4 \text{ W}$, (c) period-2 and (d) irregular pulse-train modulation at $r_1 = 53.635 \text{ mm}$ with $P_p = 4 \text{ W}$, and 4.5 W , respectively.

4.3 Spatial-temporal instability

In order to investigate the role of self-focusing effect in self-starting of the KLM laser, we focused the simulations primarily on the configuration near 1/3-degeneracy and simulated numerical evolution of laser with and without the self-focusing effect. Let the optical Kerr coefficient $n_2 = 0$, namely without the self-focusing effect, shown in Fig. 4-10(a) is a typical laser output, which always begins with a relaxation oscillation then turns to a stable output for all calculated cavity configurations at various pump

powers. The inset of Fig. 4-10(a) shows the output power versus cavity tuning region around the degenerated configuration at pump power $P_p = 4W$. It shows a power dip occurring around $r_1 = 53.625$ mm as the observation of experiment [5]. In Fig. 4-10(b), we show the numerical intensity distributions of the light fields at the beam waist inside the active medium for various cavity tuning. The field profiles show the spot size at degeneracy (labeled A) corresponding $r_1 = 53.625$ mm is smaller than that far from the degeneracy for which a $1/e^2$ spot size is defined. The spot size shrinks to approximately the pump size when the cavity is tuned toward degeneracy; it means that the gain-guiding effect dominates the transverse modes near degeneracy [17].

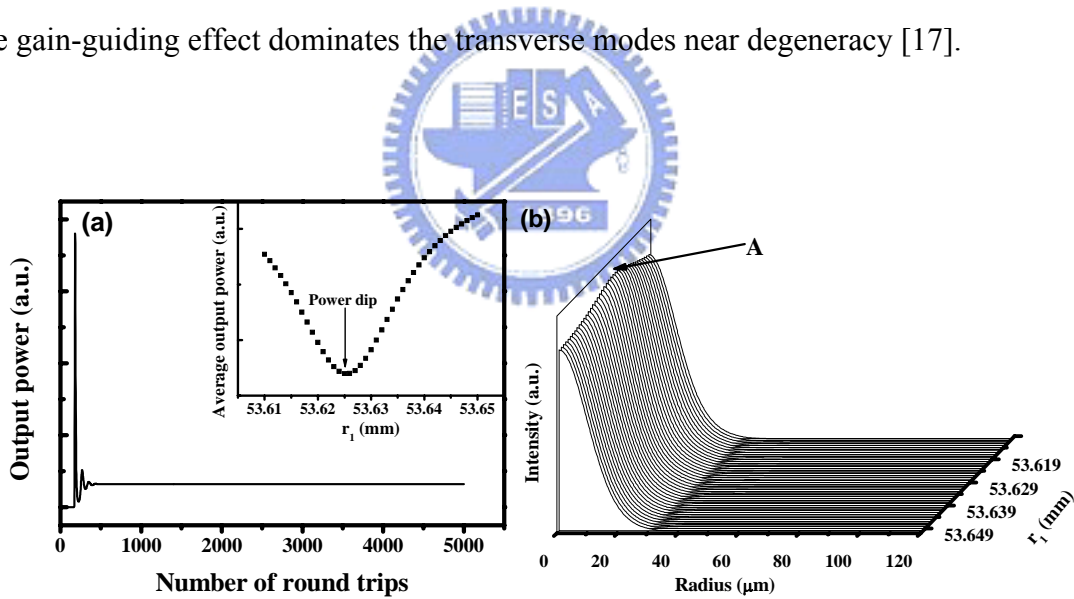


Fig. 4-10 The simulated numerical evolution of laser without self-focusing effect ($n_2 = 0$). (a) Typical laser output and the average output power versus cavity tuning region around the degenerated configuration as shown in the inset and (b) The numerical field profiles. A labeled where the degenerate cavity is.

In order to investigate the influence of the self-focusing effect, we considered $n_2 = 3 \times 10^{-20} \text{ m}^2/\text{W}$ and a pulsewidth $\tau_p = 3$ ps, and the average output power versus cavity

tuning region [see the inset of Fig. 4-3] around the degenerated configuration at $P_p = 5$. W also shows a power dip and the regions of various states for pulse-train amplitude modulation including CW or periodic state and instability such as period, period-2, irregularity, etc., which agree with the experimental observations [3]. Furthermore, Fig. 4-11 shows the temporal evolution of the intensity profiles of the period-2 pulse-train amplitude modulation (see Fig. 4-9(c)). It shows the characteristic of the spatio-temporal instability for the period-2 pulse-train amplitude modulation.

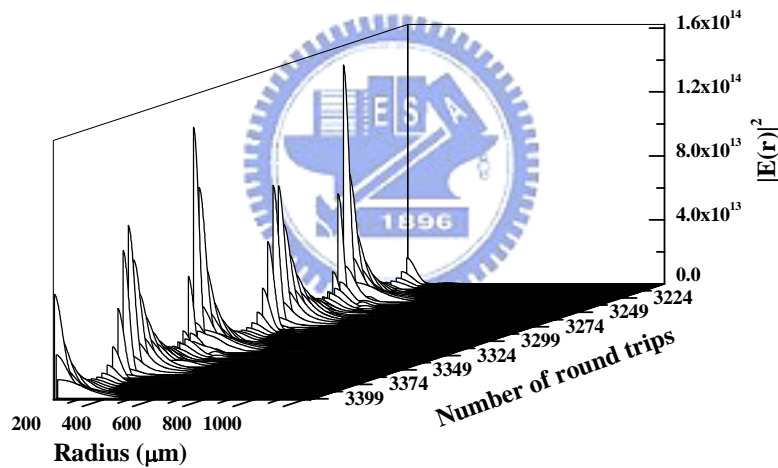


Fig. 4-11 The temporal evolution of the intensity profiles of perio-2 pulse-train amplitude modulation.

The stable laser output after the relaxation oscillation can be seen in the CW regions for the cavity tuned away from the degeneracy. However, instability output can be seen as the cavity configuration tuned close to the degenerate cavity configurations, we set here around the 1/3-transverse degeneracy, in which the transverse modes with mode numbers $m+n = 3N$ have the same frequency as the

fundamental mode, where m and n are the mode numbers of the transverse modes, and N is an integer. The laser is situated either quasi-periodic or chaotic between $r_1 = 53.63$ and 53.65 mm (solid triangles), e.g., completely chaotic at $r_1 = 53.64$ mm and at CW state (solid squares) after transient oscillation for $r_1 < 53.63$ mm and $r_1 > 53.655$ mm. It is worth noting that the simulated self-starting KLM output, as shown in Fig. 4-11 occurring around $r_1 = 53.65$ mm (open squares in the inset of Fig. 4-3), is similar to the experimental observation of continuous-wave mode-locking state, which possesses transient irregularity before reaching a constant output [4]. However, we cannot determine directly whether the constant output is completely KLM or CW output, due to lack of temporal information within a roundtrip time. Figure 4-12 shows the different runs of the simulated self-starting KLM output starting from spontaneous emission. The results reveal the laser always self-starts from irregular spiking and the irregular region changes from time to time. Because the initial field is from the spontaneous emission, the different runs have the different initial fields. Therefore the buildup time of mode-locking is sensitive to the initial condition. Other than sensitive to the initial conditions, we further numerically calculated the buildup times of self-starting mode-locking at $r_1 = 53.65$ mm with 2,000 times. Figure 4-13 shows a histogram of the numerically measured self-start times (solid squares). The distribution of buildup time of self-starting mode-locking shows a tendency with the

exponential decay (dash line) similar to the self-starting behavior in an additive-pulse mode locked fiber laser [39] and previous theoretical result [40].

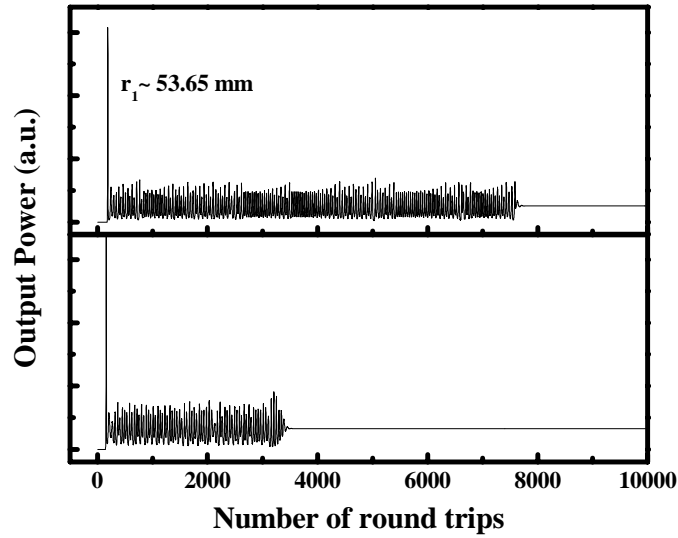


Fig. 4-12 The evolution of laser from two different runs show both starting from the irregular spiking before reaching a periodic (KLM) state around $r_1=53.625$ mm.

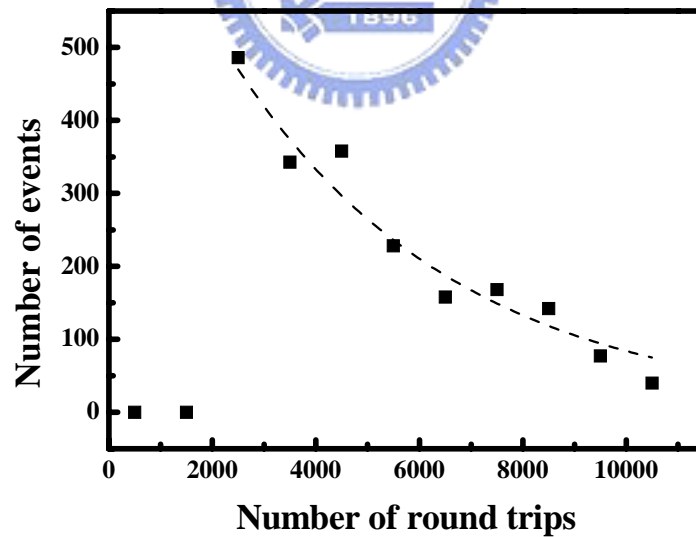


Fig. 4-13 The histogram of the calculated buildup times of self-starting mode-locking (solid squares) with an exponential fitting curve (dash line).

References

- [1] C. C. Hsu, J. H. Lin, and W. F. Hsieh, *Appl. Phys. B* **96**, 401 (2009).
- [2] P. Grassberger, and I. Procaccia, *Phys. Rev. Lett.* **50**, 346 (1983).
- [3] C. C. Hsu, J. H. Lin, and W. F. Hsieh, *J. Phys. B* **42**, 145402 (2009).
- [4] C. C. Hsu, C. H. Chen, and W. F. Hsieh, *J. Phys. B* **submitted** (2009).
- [5] J. H. Lin, M. D. Wei, and W. F. Hsieh, *J. Opt. Soc. Am. B* **18**, 1069 (2001).
- [6] J. H. Lin, and W. F. Hsieh, *Opt. Commun.* **225**, 393 (2003).
- [7] H. Haken, *Phys. Lett. A* **53**, 77 (1975).
- [8] H. Risken, and K. Nummedal, *J. Appl. Phys.* **39**, 4662 (1968).
- [9] R. Graham, and H. Haken, *Z. Phys.* **213**, 420 (1968).
- [10] L. A. Lugiato, C. Oldano, and L. M. Narducci, *J. Opt. Soc. Am. B* **5**, 879 (1988).
- [11] A. E. Siegman, *Lasers* (University Science Books, Mill Valley, California, 1986).
- [12] S. A. Collins, *J. Opt. Soc. Am.* **60**, 1168 (1970).
- [13] C. H. Chen, M. D. Wei, and W. F. Hsieh, *J. Opt. Soc. Am. B* **18**, 1076 (2001).
- [14] S. R. Bolton, and M. R. Acton, *Phys. Rev. A* **6206** (2000).
- [15] N. H. Packard, J. P. Crutchfield, J. D. Farmer, and R. S. Shaw, *Phys. Rev. Lett.* **45**, 712 (1980).
- [16] H. Haken, *Synergetics: An Introduction* (Springer, Berlin, 1985).

- [17] C. H. Chen, P. T. Tai, W. F. Hsieh, and M. D. Wei, *J. Opt. Soc. Am. B* **20**, 1220 (2003).
- [18] P. T. Tai, and W. F. Hsieh, *Opt. Express* **13**, 1679 (2005).
- [19] M. C. Cross, and P. C. Hohenberg, *Rev. Mod. Phys.* **65**, 851 (1993).
- [20] P. Melby, J. Kaidel, N. Weber, and A. Hubler, *Phys. Rev. Lett.* **84**, 5991 (2000).
- [21] A. Yariv, *Optical Electronics* (Saunders College, 1991).
- [22] J. M. Shieh, F. Ganikhanov, K. H. Lin, W. F. Hsieh, and C. L. Pan, *J. Opt. Soc. Am. B* **12**, 945 (1995).
- [23] D. Y. Tang, M. Y. Li, N. R. Heckenberg, and U. Hubner, *J. Opt. Soc. Am. B* **13**, 2055 (1996).
- [24] J. H. Lin, W. F. Hsieh, and H. H. Wu, *Opt. Commun.* **212**, 149 (2002).
- [25] J. N. Kutz, B. C. Collings, K. Bergman, and W. H. Knox, *IEEE J Quantum Electron.* **34**, 1749 (1998).
- [26] H. A. Haus, *IEEE J Quantum Electron.* **12**, 169 (1976).
- [27] Y. M. Liu, and P. R. Prucnal, *IEEE Photon. Technol. Lett.* **5**, 704 (1993).
- [28] Q. R. Xing, W. L. Zhang, and K. M. Yoo, *Opt. Commun.* **119**, 113 (1995).
- [29] F. T. Arecchi, R. Meucci, G. Puccioni, and J. Tredicce, *Phys. Rev. Lett.* **49**, 1217 (1982).
- [30] C. O. Weiss, and W. Klische, *Opt. Commun.* **51**, 47 (1984).

- [31] C. O. Weiss, and R. Vilaseca, *Dynamics of Lasers* (Weinheim; New York; Basel; Cambridge: VCH 1991).
- [32] L. A. Lugiato, F. Prati, L. M. Narducci, P. Ru, J. R. Tredicce, and D. K. Bandy, *Phys. Rev. A* **37**, 3847 (1988).
- [33] L. A. Lugiato, G. L. Oppo, J. R. Tredicce, L. M. Narducci, and M. A. Pernigo, *J. Opt. Soc. Am. B* **7**, 1019 (1990).
- [34] G. Dalessandro, and G. L. Oppo, *Opt. Commun.* **88**, 130 (1992).
- [35] C. H. Chen, P. T. Tai, and W. F. Hsieh, *Opt. Commun.* **241**, 145 (2004).
- [36] H. H. Wu, and W. F. Hsieh, *J. Opt. Soc. Am. B* **18**, 7 (2001).
- [37] H. H. Wu, C. C. Sheu, T. W. Chen, M. D. Wei, and W. F. Hsieh, *Opt. Commun.* **165**, 225 (1999).
- [38] P. T. Tai, W. F. Hsieh, and C. H. Chen, *Opt. Express* **12**, 5827 (2004).
- [39] B. Vodonos, A. Bekker, V. Smulakovsky, A. Gordon, O. Gat, N. K. Berger, and B. Fischer, *Opt. Lett.* **30**, 2787 (2005).
- [40] A. Gordon, O. Gat, B. Fischer, and F. X. Kartner, *Opt. Express* **14**, 11142 (2006).



Chapter 5 Conclusions and Prospective

5.1 Conclusions

In this dissertation, we have observed self-starting Kerr-lens mode-locking with picosecond pulses in the Ti:sapphire laser without external modulation and feedback control. To understand how the KLM laser self starts from spontaneous emission and then transfers to mode-locking, we have analyzed the transient irregularity of the laser output before the complete mode locking by using nonlinear analysis. Because the correlation dimension is a finite and non-integer value it indicates the transient irregularity is chaotic. From the decay autocorrelation function with long time revival, we ascertained further that the SSKLM is initially at the chaotic state. Based on the Fox-Li approach, including the self-focusing effect, the simulation results reveal that the self-focusing effect is responsible for the dynamics of this laser system that evolves from the chaotic state with a strange attractor to a quasi-periodic state, and then converges to a fixed point. After long time evolution, the nonlinear Kerr coefficient γ does adapt to the edge of chaos.

Furthermore, we have also observed slow pulse-train amplitude modulation phenomena in a self-mode-locked picosecond Ti:sapphire laser. Periodic pulse-train modulation appeared when pump power reached 4 W. As the pump power is

increased further, each modulation envelope splits into two or three clusters with increasing modulation depth; and the laser would eventually lead to irregular modulation pulse train if the pump power is increased even further. The observed irregular pulse envelope modulation is spatio-temporal with non-stationary transverse pattern. The slow amplitude modulation should be supported by exciting two sets of non-degenerate longitudinal mode-locked supermodes due to spatially inhomogeneous gain modulation in the Ti:sapphire crystal.

Finally, we use numerical model to investigate the dynamics in a Kerr-lens mode-locked laser with and without the self-focusing effect around the 1/3-degenerate cavity configuration. Typical laser output always begins with a relaxation oscillation then turns to a stable output for all calculated cavity configurations at various pump powers without self-focusing effect. The feature of a power dip, which is due to the spot size shrinkage at the degeneracy, agrees with the observation of experiment. However, with considering the self-focusing effect, the output power versus cavity tuning region around the degenerated configuration shows not only a power dip but various states including continuous-wave or periodic state and instability for pulse-train amplitude modulation such as period, period-2, and irregular states, etc. The simulated self-starting KLM, which possesses transient irregularity before reaching a constant output, occurs between the instability and CW region. Furthermore, the different runs

of the simulated self-starting KLM output starting from spontaneous emission reveal the laser always self-starts from irregular spiking and the irregular region changes from time to time. Therefore the buildup time of mode-locking is sensitive to the initial condition and its distribution shows the exponential decay.

5.2 Prospective

In this dissertation we have experimentally and numerically studied the nonlinear dynamics of the ps KLM laser around the 1/3-degenerate cavity configuration. However, because the behaviors of laser dynamics depends on the nonlinearity around the degenerated cavity configurations, the experimental observation of the other degenerated cavity configurations such as $G_1G_2 = 1/2, 3/4$, etc. will be the next aim of study. Besides, considering the dispersion compensation in KLM lasers, the pulse width of mode-locked pulses can be reduced to several tens femtosecond, the modulation depth of pulse-train amplitude modulation may be deeper than that in the ps KLM laser and then it may form a Q-switched mode-locked laser.

In our simulated model we only considered the spatial effects, but neglected the temporal effects such as the dispersion in the gain medium and assumed that the pulse width does not change for propagating in the laser cavity. In fact, because the pulse width would change with the formation of pulse, the dispersion should be considered in our model. Hence, we can obtain the information of pulse width by using the temporal

ABCD matrices when pulses propagate through gain medium. If we do so, the computation will consume more time than our simulated model and a computer cluster should be needed.



簡歷

姓名：許智章

性別：男

出生年月日：62年02月23日

學歷：

學校 / 科系	學位	起訖年月
交通大學 / 光電所	博士	2001年09月 ~ 2009年06月
交通大學 / 光電所	碩士	1996年09月 ~ 1998年06月
東海大學 / 物理系	學士	1992年09月 ~ 1996年06月

經歷：

服務單位	職位	起訖年月
東海大學物理系	專任助教	2000年08月 ~ 2001年07月

著作目錄

一、期刊論文

- [1] **Chih-Chang Hsu**, Chen-Hsu Chen, Wen-Feng Hsieh, "Suppressing chaos to complete Kerr-lens mode-locked laser," Submitted to J. Phys. B (2009).
- [2] **Chih-Chang Hsu**, Ja-Hon Lin and Wen-Feng Hsieh, "Adaptation to the edge of chaos in a self-starting Kerr-lens mode-locked laser," Submitted to Appl. Phys. B **96**, 401 (2009).
- [3] **Chih-Chang Hsu**, Ja-Hon Lin, and Wen-Feng Hsieh, "Pulse-train modulation in a picosecond self-mode-locked laser," J. Phys. B: At. Mol. Opt. Phys. **42**, 145402 (2009).

- [4] Yun-Pei Chan, Ja-Hon Lin, **Chih-Chang Hsu**, and Wen-Feng Hsieh, “Near-resonant high order nonlinear absorption of ZnO thin films,” *Opt. Express* **16**, 19900 (2008).
- [5] **Chih-Chang Hsu**, Ja-Hon Lin, Ying-Shu Chen, Ying-Hsiu Lin, Hao-Chung Kuo, Shing-Chung Wang, Wen-Feng Hsieh, Nelson Tansu and Luke J Mawst, “Ultrafast carrier dynamics of InGaAsN and InGaAs single quantum wells,” *J. Phys. D: Appl. Phys.* **41**, 085107 (2008).
- [6] Ja-Hon Lin, Kuei-Huei Lin, **Chih-Chang Hsu**, Wen-Hsun Yang, and Wen-Feng Hsieh, “Supercontinuum generation in a microstructured optical fiber by picosecond self Q-switched mode-locked Nd:GdVO4 laser,” *Laser Phys. Lett.* **4**, 413 (2007).
- [7] Ja-Hon Lin, **Chih-Chang Hsu**, Wen-Feng Hsieh, Kuei-Huei Lin, “Build-up of supercontinuum in heated and unheated photonic crystal fibers using a chirped femtosecond laser,” *Opt. Commun.* **265**, 659 (2006).

二、會議論文

- [1] **Chih-Chang Hsu**, Ja-Hon Lin, and Wen-Feng Hsieh, “Suppressing chaos to complete Kerr-lens mode-locking in a self-starting Kerr-lens mode-locked laser,” in Conference of Year 2008 Annual Meeting of Chinese Physical Society, Hsinchu, TAIWAN, aE-02 (2008).
- [2] Yin-Su Chen, **Chih-Chang Hsu**, Hsin-Ming Cheng, and Wen-Feng Hsieh, “The ultrafast dynamics of InAs quantum dots probed by femtosecond spectroscopy,” in Conference of Year 2007 Annual Meeting of Chinese Physical Society, Chung-Li, TAIWAN, dE2-03 (2007).
- [3] Wen-Feng Hsieh, **Chih-Chang Hsu**, Ja-Hon Lin, “Adaptation to the edge of chaos in a self-starting soft-aperture Kerr-lens mode-locked laser,” *Frontiers in Optics 2007/Laser Science XXIII conferences*, San Jose, California, USA, FWC8 (2007).
- [4] **Chih-Chang Hsu**, Ja-Hon Lin, Ying-Hsiu Lin, and Wen-Feng Hsieh, “The ultrafast time-resolved photorefectance measurement of $\text{In}_{0.4}\text{Ga}_{0.6}\text{As}_{1-x}\text{N}_x$ single quantum well,” in Conference of Year 2006 Annual Meeting of Chinese Physical Society, Taipei, TAIWAN, BG-07 (2006).

- [5] **Chih-Chang Hsu**, Ja-Hon Lin, and Wen-Feng Hsieh, “Amplitude modulation of picosecond pulse-train in self-mode-locked Ti:sapphire laser,” in Proceedings of Optics and Photonics Taiwan'03, Taipei, TAIWAN, (2003).